Comparison of the Highly Reflective Cloud and Outgoing Longwave Radiation Datasets for Use in Estimating Tropical Deep Convection

DUANE E. WALISER*

California Space Institute, Scripps Institution of Oceanography, University of California at San Diego, La Jolla, California

NICHOLAS E. GRAHAM

Climate Research Division, Scripps Institution of Oceanography, University of California at San Diego, La Jolla, California

CATHERINE GAUTIER

Earth Space Research Group, University of California at Santa Barbara, Santa Barbara, California

(Manuscript received 14 October 1991, in final form 2 March 1992)

ABSTRACT

Currently, there are two long-term satellite-derived datasets most are frequently used as indices for tropical deep convection. These are the Outgoing Longwave Radiation (OLR) and Highly Reflective Cloud (HRC) datasets. Although both of these datasets have demonstrated their value, no direct comparison of these datasets has been conducted, to determine how well they agree when used to estimate tropical convection, nor has there been much work toward comparing these long-record datasets with more recently developed convection datasets. This information is vital since the inhomogeneous sampling of the in situ rainfall record makes it inadequate for many studies concerning tropical convection and the more modern datasets have not achieved a climatologically useful record length for all studies. The goal of this paper is to compare these two datasets in order to quantify their strengths and weaknesses. This information will provide guidance in choosing the most appropriate dataset(s) for subsequent studies, interpreting the results from those studies, and extending more modern convection datasets backward.

Comparisons are done in terms of their climatological and frequency-dependent characteristics, their consistency in identifying deep tropical convection, and their relationships to local sea surface temperature (SST). Additionally, use is made of the more modern, shorter-term International Satellite Cloud Climatology Project stage C2 dataset as a means of further comparison and validation. The results of this study reveal some important differences between the HRC and OLR in terms of their temporal and spatial scales of variability, their relationships to other geophysical fields, and the logistics of their use. Further, they suggest that for many applications the HRC more accurately represents the characteristics of cloud cluster–scale tropical convection. This is especially true in cases where 1) characterization of the spatial scales or frequency-dependent variability of convection is important, 2) the relationships between deep convection and SST or water vapor are being considered, and 3) the domain of interest is large enough to contain spatial inhomogeneities, such as land–sea contrasts or inhomogeneous SST and moisture fields.

One new and important finding of this study is that both the OLR–SST and HRC–SST relationships show that SSTs in excess of about 29.5°C tend to occur only under conditions of diminished convection. Thus, the maximum convective activity does not occur over the *warmest* (>29.5°C) water; rather, the warmest water occurs under "clear," less-convective skies. Further, our results empirically demonstrate that in a highly convective regime the maximum equilibrium SST that can be supported is about 29.5°C. These results are further evidence that convective-cloud complexes provide a systematic and climatologically important cooling effect on the surface temperature.

1. Introduction

The emergence of the satellite era produced the capability to estimate tropical convection on a wide range of temporal and spatial scales. The long-term (> ~10 yr) availability of these satellite measurements and their derived products has produced what arguably could be our best climatology of tropical convection and has led to significant progress in the understanding of many aspects of tropical convection, ranging from El Niño to cumulus-scale phenomena. Despite the great progress resulting from these observations, shortcomings still exist in our ability to determine cloud properties and make accurate estimates of precipitation from these satellite measurements (see Rossow 1989; Arkin and Ardanuy 1989). The ship and land-based precipitation climatology suffers from very inhomogeneous sampling

* *Present affiliation:* Department of Atmospheric Sciences, University of California, Los Angeles.

Corresponding author address: Dr. Duane E. Waliser, 7127 MS Building/Mail Code 156505, Department of Atmospheric Sciences, University of California, Los Angeles, Los Angeles, CA 90024-1565.

characteristics and is therefore inadequate for many tropical convection studies. For these reasons, there is an essential need to understand the available long-term, remotely sensed indices of tropical convection and to quantify their strengths and weaknesses.

Currently, two long-term satellite-derived datasets are most frequently used for climatological studies of tropical convection. These are the Outgoing Longwave Radiation (OLR) dataset and the Highly Reflective Cloud (HRC) dataset. The OLR data have been used extensively to study the El Nino–Southern Oscillation phenomena (e.g., Gill and Rasmusson 1983; Rasmusson and Wallace 1983; Lau and Chan 1988) and the intraseasonal/30–60-day oscillation (e.g., Weickmann 1983; Weickmann et al. 1985; Lau and Chan 1985, 1986a, 1986b; Knutson and Weickmann 1987) and to make estimates of tropical precipitation (Arkin 1984; Morrissey 1986; Yoo and Carton 1988). The relationships between large-scale characteristics of convection, sea surface temperature (SST), and wind divergence have been examined by a number of investigators using OLR (e.g., Graham and Barnett 1986; Gutzler and Wood 1990). The OLR data has also been used in tropical circulation studies (e.g., Liebmann and Hartmann 1982) as well as regional climate studies (e.g., Horel et al. 1989). The HRC data have been used less frequently than OLR but have also been employed in ENSO studies (e.g., Ramage and Hori 1981), precipitation estimates (Kilonsky and Ramage 1976; Garcia 1981), and studies addressing general characteristics of large-scale convection (Zimmerman et al. 1988; Hastenrath 1990). Zebiak (1990) has compared both the HRC and OLR datasets to model-inferred atmospheric forcing and found slightly better agreement using the HRC (Zebiak, personal communication 1991).

Although both the HRC and OLR datasets show clear value, no direct comparison of these two datasets has been conducted to determine how well they agree when used to estimate deep convection, nor has there been much work toward comparing these long-record datasets with more recently developed convection datasets [e.g., International Satellite Cloud Climatology Project (ISCCP), see Rossow et al. (1991)]. Furthermore, since there are no homogeneous, large-scale in situ measurements of tropical convection, it is worthwhile to "validate" these datasets through an intercomparison. This paper presents the findings of such a comparison. It is hoped that the results in this study will help guide investigators interested in applying these long-term datasets to studies concerning tropical convection and help guide in the extension of the more modern, shorter-term satellite convection index datasets (e.g., ISCCP, Special Sensor Microwave Imager) backward to build a longer-term and more accurate climatology of deep convection and/or precipitation.

The comparative analysis of these datasets performed in this study is based on an understanding of the fundamental processes associated with deep convection in the tropics and, in particular, the view of these processes from space. The analysis includes 1) direct comparisons between the HRC and OLR, 2) comparisons of the HRC and OLR to other cloud/convection data products, and 3) a comparison of their relationship to a third important variable in the climate system, particularly for the forcing of convection, SST. The paper is organized as follows. Section 2 provides a description of the datasets and analysis methods used in this study. Section 3 provides a brief description of the deep convection process and its view from space. Section 4 compares the climatological characteristics, frequency-dependent variability, and coherence of the HRC and OLR datasets. Section 5 utilizes the more recent ISCCP C2 dataset as means for further comparison and validation of the two datasets. Section 6 compares the relationships of HRC and OLR to local absolute SSTs and local SST anomalies. Section 7 presents a summary of the results.

2. Data and analysis methods

a. HRC

The original concept behind the HRC was developed by Kilonsky and Ramage (1976), who used subjectively analyzed visible satellite mosaics (daytime only) to identify the frequency of occurrence of highly reflective clouds and infer rainfall rates over the tropical Pacific. This inference is plausible since the cloud reflectivity is principally due to the liquid water content in the cloud. Their method of determining "highly reflective clouds" (or highly precipitating clouds) was improved upon by Garcia (1985), who, in addition to using the visible mosaics, analyzed the infrared mosaics as well to filter out low- and midlevel highly reflective clouds. Therefore, the name "highly reflective high clouds" would be more suitable in describing the cloud types identified as HRC.

Garcia (1985) used this method to create the long-term HRC dataset. The production of this dataset was a formidable task motivated by the desire to create a long-term dataset that identifies cloud cluster–scale convection and filters out low-level stratus (using the IR mosaics) and thin cirrus clouds (using the visible mosaics). The dataset is composed of daily "images" of ones and zeros, where ones identify regions of "deep, organized tropical convective systems extending at least 200 km horizontally, each being composed of many individual convective cells embedded within a common cirrostratus canopy" (Garcia 1985). The spatial resolution of the HRC dataset is $1° \times 1°$ and extends from 25°N to 25°S and from 0° to 359°E.[1] This daily

[1] Note: the HRC dataset resolves convective cloud clusters at a 1° resolution; however, an HRC-convective event is defined only when the cloud cluster is larger than 200 km in one horizontal dimension. In this paper, the data have been mapped to a 2° grid for comparison, and the "characteristic" scale of the HRC is taken to be order 200 km.

dataset currently extends from January 1971 to December 1987 (IR mosaics were not utilized until 1974). In addition to the data grid, a separate grid is also provided for each daily image identifying areas of missing data.

Our analysis of the dataset showed that the total amount of missing data is about 5% over a majority of the tropics. The continuity of the dataset is exceptionally good, with the length of the longest time gap at any one grid point generally between 4 and 7 days, with the longest gap in the entire dataset being 15 days over a very small region near the date line.[2] Further, 70% of the total missing data points is composed of gaps with lengths of only 1 day, and 10% comes from gap lengths of 2 days.

b. OLR

The OLR dataset used in this study was constructed by Horel and Cornejo-Garrido (1986). This dataset was produced from daytime and nighttime archived OLR estimations (W m^{-2}; see Gruber and Krueger 1984), interpolated onto a 2° × 2° grid between 30°N and 30°S from 1°E to 1°W, and then time-averaged into 5-day means. The dataset extends from June 1974 to May 1988 with gaps of 10 months during 1978, 2 months during 1987, and 3 other missing pentads.

c. ISCCP C2 and SST

This ISCCP stage C2 dataset (Rossow et al. 1991; Rossow and Schiffer 1991) contains monthly averages of derived cloud types in terms of their frequency of occurrence, cloud-top temperatures, and cloud-top pressures, along with other auxiliary information and data products at 2.5° resolution. All derived cloud types are based on cloud-top pressure and optical thickness, and are mutually exclusive (see Fig. 2.2 of appendix C of Rossow et al. 1991). These cloud types are assigned from daytime observations only and have a sampling interval of 3 hours. The deep convective cloud type has been assigned to observations when the optical thickness has a value greater than 23 and when the cloud-top pressure is less than 440 mb. This classification indicates very deep (or thick) clouds with high cloud tops. In the sense that optically bright high clouds are so designated, the ISCCP C2 method is an objective analog to the subjective approach used in defining HRC. The specific C2 data quantity used in this study as an index of deep convection is the frequency of the deep convective cloud type (hereafter C2-DC). It is computed from the fraction of subsampled pixels in an equal-area grid box that indicate deep convection for a particular month. The pixel size ranges between about 4 and 8 km for nadir viewing, depending on the satellite. The equal-area grid box has a 2.5° resolution at the equator. The subsampling interval is about 25 to 30 km depending on the satellite. Also used in this study from the C2 dataset are the Tiros Operational Vertical Sounder (TOVS) water vapor retrievals and the frequency of total middle- and total high-level clouds (deep convective clouds are one of three categories of high-level clouds). At the time of this study's analysis, 30 months (July 1983 to December 1985) of ISCCP C2 data were available.

The monthly mean SST observations used in section 5b and section 6 are from the Climate Analysis Center satellite–in situ blended SST dataset (Reynolds 1988).

d. Analysis domain

All analysis of the HRC, OLR, and ISCCP C2 data were performed using 2° × 2° gridded data over the global tropical region, from 25°N to 25°S. The analyses using pentad data (section 4) required remapping the daily HRC data onto the 2° × 2° grid and counting over the same 5-day time periods used in the OLR dataset (giving days/pentad). The analyses using monthly data (sections 5 and 6) required averaging the OLR pentads into monthly means, and remapping the monthly 1° × 1° HRC (in days/month) and 2.5° × 2.5° ISCCP C2 grids to the 2° × 2° resolution grid.

e. Fourier analysis methods

The power spectra in section 4b were computed by Fourier transforming the time-lagged autocorrelations at each point of the study domain (Bendat and Piersol 1986). The autocorrelations were computed using up to 256 time lags of the 5-day data. The coherences in section 4c were computed from the Fourier-transformed autocorrelations and cross correlation of the HRC and OLR data using the same 256 time lags. In all cases of auto and cross correlations, a Bartlett window was applied to the correlations before transforming. Since the comparisons in these sections were based on the average signal over five characteristic time scales, this method of time-scale decomposition was found to be adequate for the purposes of this study. Not all time series and/or periodic phenomenons, however, lend themselves well to Fourier decomposition, and the shortcomings of this method are pointed out in the text where they exist and were found to influence the results.

3. Satellite observations of tropical convection

To better understand how the HRC and OLR relate to each other in terms of their ability to serve as proxies for convection observations, it is useful to describe the systems that make up deep convection in the tropics and infer their effect on radiation at the top of the atmosphere, the parameter measured from the satellite.

[2] Optical Line Scanner (OLS) data from the Defense Meteorological Satellite Program (DMSP) satellites was used to fill in the gaps in the NOAA satellite series during 1978.

Briefly, large-scale convective systems are generally composed of a number of developing and decaying mesoscale precipitating features (MPFs) embedded in a common cirrostratus canopy (Leary and Houze 1979; Houze and Betts 1980). The evolution of these MPFs usually begins as a loosely organized set of convective cells. These cells develop vertically into the upper troposphere concurrently with the formation of a precipitating anvil cloud near the top of the convective cells. This anvil cloud extends leeward of the upper-level winds and spreads into a much larger region of cirrostratus cloud. In the dissipating stage, the anvil cloud persists for several hours after the cessation of new convective cell formation while the cirrus cloud can persist considerably longer. The synoptic conditions favorable for convective activity can persist for days, but the individual mesoscale features are much shorter lived ($\sim$1 day). Typical spatial scales for convective cells are about $1–10^2$ km^2, for MPFs about $10^2–10^4$ km^2, and for cloud clusters about $10^4–10^6$ km^2.

The radiative properties of these cloud elements as observed by satellites depend on the distribution of cloud liquid water in clouds for the reflected solar measurements and on cloud-top temperature for the infrared measurements. Both microphysical properties such as drop sizes and macroscopic properties such as optical depth, cloud height, and horizontal extent affect their radiative properties (e.g., Aida 1976; Welch and Zdunkowski 1981; Fouquart 1985). Further, in most interpretations of satellite observations, it is implicitly assumed that the cloud target viewed by the satellite is a solid, uniform, dense layer. In fact, the cloud field may be broken or scattered, and the satellite sensor will measure a radiance that is a combination of cloud and the darker and warmer background surface (the ocean surface). Radiances from broken cloud fields have been found to be extremely difficult to interpret in terms of cloud physical properties (e.g., Coakley and Davies 1986; Davies 1984; Harshvardhan 1982).

In view of these characteristics of tropical convective systems, an attempt can be made to interpret and determine the characteristics of the HRC and OLR data. HRC is computed from the number of days over a period of several days an area with a 200-km extent is covered with clouds of high reflectance and low infrared values (subjectively determined). It thus represents a time-weighted coverage. Because the typical lifetime and spatial scale of MPFs are smaller than those of tropical cloud clusters, it can be realized that some MPFs will be missed by the HRC analysis, particularly those that are in the development phase, whereas well-defined (even decaying) cloud clusters will be definitely counted. Thus, in general, there will be some contrast in the dataset, that is, spatial variability in the visible brightness field at a scale smaller than that analyzed. In contrast to HRC, OLR data represent a mean temperature averaged over the time period analyzed. Because the vertical temperature profile near the tropopause (to which MPFs extend) is relatively invariant with height, it is expected that the infrared radiance field will be spatially homogeneous, despite the differences in altitude between the top of the active MPFs and the cirrus anvil of dissipating MPFs. So, overall, HRC is expected to have higher spatial variability than OLR. Furthermore, since a large part of a cloud cluster's life cycle is spent in a stage of dissipation (i.e., well-formed anvil) by contrast with the time spent in a stage of formation (i.e., growing precipitation cells), it is expected that, overall, the analysis of OLR data could indicate more extensive coverage, in both time and space, than does the analysis of HRC data. Both of these inferences are found to be the case in the results of the next sections.

4. Direct HRC and OLR comparisons

This section addresses the climatological characteristics of the two datasets including their temporal and spatial decorrelation scales, frequency-dependent variability, and coherence. All results in this section use the 5-day values of HRC and OLR from their overlapping periods (essentially 1974–1987). The comparisons done in this section show that although both datasets indicate similar spatial distributions of mean deep tropical convection, there are differences in the spatial distribution of variance and in the frequency-dependent characteristics of the datasets.

a. Climatological characteristics

Figure 1 displays the overall long-term mean HRC and OLR fields based on 5-day data. The mean HRC values range between 0.0 and 1.2 days/pentad, while the OLR values range between 300 and 200 W m^{-2}. The two maps show the same structure, with each depicting the intertropical convergence zones (ITCZs), the South Pacific convergence zone (SPCZ), the intense convection over the tropical continents of Africa and South America, and the convection near the monsoon regions of southern Asia, northern Australia, and Central America. The only major difference between the two distributions is the contrast between the structures away from the equator at the northern and southern edges of the tropics. The HRC shows zero values in these regions since deep tropical convection seldom occurs in the subtropics. The OLR on the other hand, shows some structure north and south of the ITCZ and off the coasts of the tropical continents since it is directly influenced by the spatial distributions of SST, moisture, and nonconvective cloud cover, as well as the distribution of deep convection. More detailed analysis concerning the sensitivity of OLR and HRC to quantities other than deep convection is performed in section 5b.

Figure 2 displays the overall long-term standard deviations of the HRC and OLR based on 5-day data.

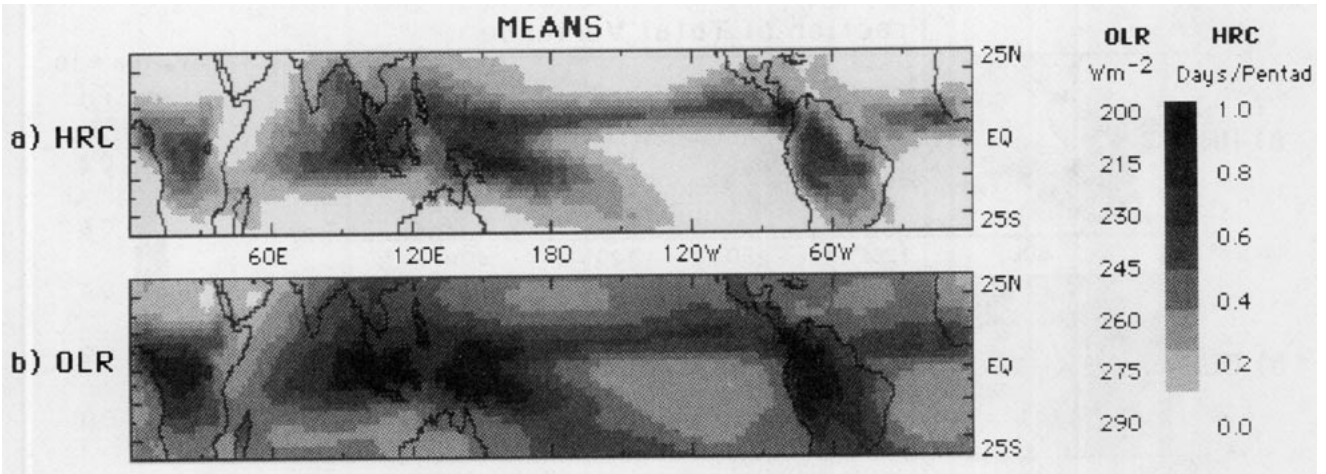

FIG. 1. Mean maps of HRC (a) and OLR (b). Means were produced from 5-day averages from 1974 to 1987.

Again the spatial structures are very similar. Although these two figures are not directly comparable because the units are different, they are included for the sake of completeness in presenting a comparison of the climatologies of the datasets. The standard deviation of the HRC ranges between 0.0 and 1.0 days/pentad. The standard deviation of the OLR ranges between about 6 and 48 W m^{-2}. For a more direct (albeit arbitrary) comparison of variance, Fig. 3 shows a normalized version of the variance fields. In this figure, the variance at each point is normalized by the total variance in the entire field. The most dramatic difference between these two maps is that the variance in the HRC field is more tightly confined to the convergence zones than the variance of the OLR. In fact, the spatial structure of the former is nearly identical to the mean HRC. The OLR variance distribution, however, is much smoother, indicating larger spatial scales of variation (cf. Fu et al. 1990).

The broader spatial scales of the OLR noted above are readily seen from the spatial autocorrelations shown in Fig. 4. This plot shows the HRC and OLR zonal autocorrelations. These were computed by ensemble averaging the zonal autocorrelation of each zonal strip in the region 10°N to 10°S between 60°E and 180° for each time period (pentad). Using a characteristic decorrelation value of $1/e$, this plot shows that the spatial scales of the OLR are broader than that of the HRC. For 5-day time scales, the decorrelation distance is about 1400 km for the OLR and about 800 km for the HRC. The temporal autocorrelations (not shown), computed by ensemble averaging the temporal autocorrelations of each point in this domain, were very similar with the HRC having a slightly smaller decorrelation scale. This contrast in decorrelation scales is highly dependent on the averaging period. As expected, and from the discussion in section 3, the contrast will be larger for daily time scales, while for monthly and

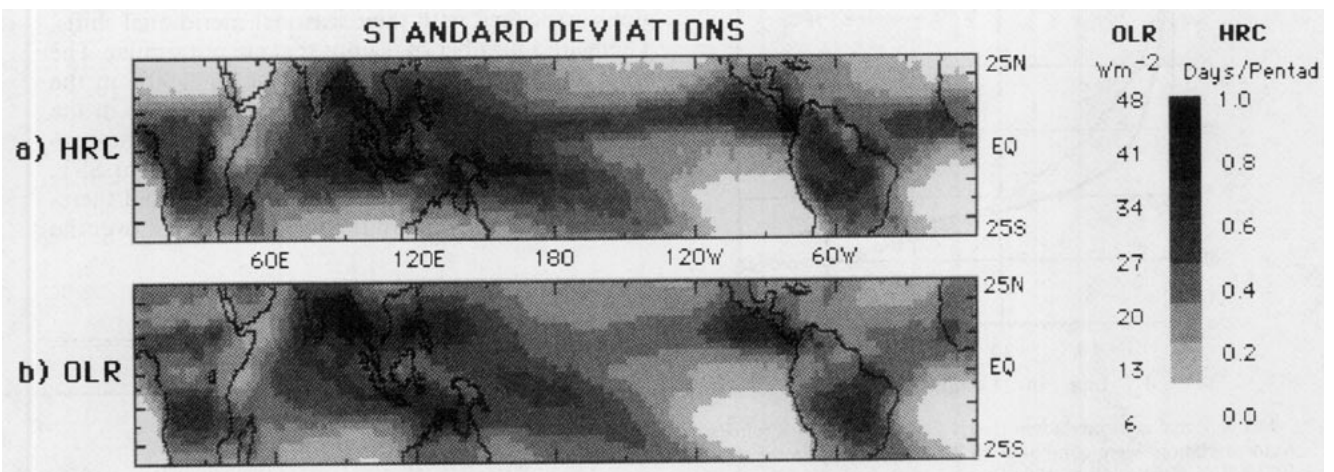

FIG. 2. Standard deviations of HRC (a) and OLR (b). Standard deviations were produced from 5-day averages from 1974 to 1987, and are computed about the means shown in Fig. 1.

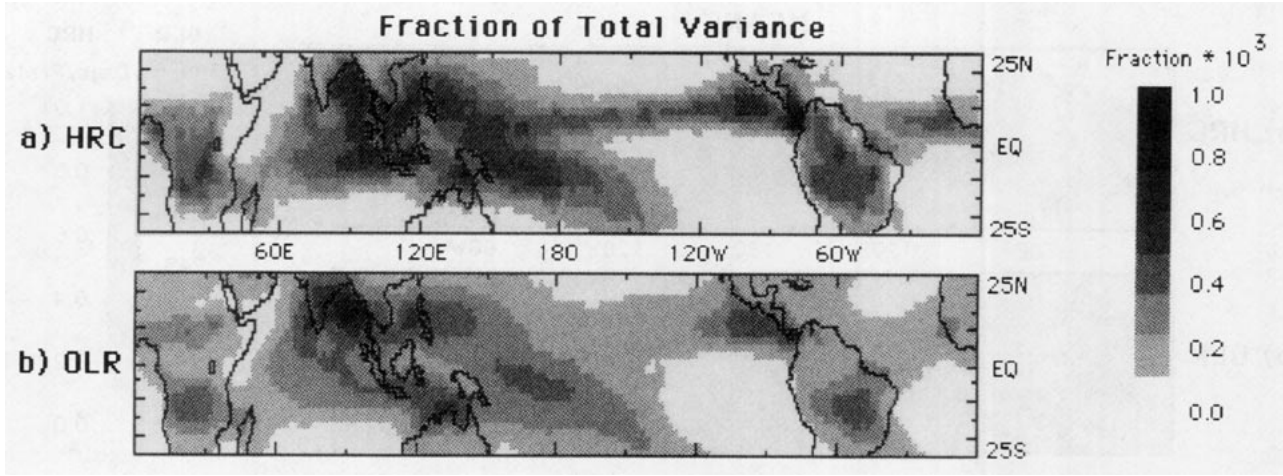

FIG. 3. Fraction of total variance of (a) HRC and (b) OLR. These variance maps were computed by normalizing the standard deviations shown in Fig. 2 by the total variance of the entire field.

longer time scales, the decorrelation scales become more similar.

b. *Frequency-dependent variability*

To determine the spatial structure of the frequency-dependent variability, normalized power spectra of OLR and HRC were calculated for each point in the study domain (see section 2e). The fraction of total variance for each of the five time scales delineated in Table 1, is mapped in Figs. 5 (HRC) and 6 (OLR). It can be seen that for each field the main region of interannual variance occurs in the central Pacific where the interannual El Nino–Southern Oscillation (ENSO) phenomena have the most dramatic impact on convection and sea surface temperatures. The contribution to the variance from the interannual time scale in this region is less in the HRC dataset than in the OLR dataset, about 20%–30% for the HRC and 40%–50% for the OLR. In addition, the OLR shows other areas where about 10% or more of the variance occurs at interannual time scales: for example, the northeast Pacific, northern Africa, and along and off the western coasts of South America and Africa. The interannual variance in these regions is primarily due to changes in SST, moisture, and nonconvective cloud cover, and therefore, does not show up in the HRC data.

With respect to the annual cycle, the OLR (Fig. 6b) has large fractions of variance at the annual time scale, as great as 60% over continental regions and near strong monsoon regimes. The HRC map (Fig. 5b) shows a similar spatial structure of variance at the annual time scale, although the contributions to the total variance are only about 30%. Both datasets contain annual cycle contributions at the edges of the major convective regions associated with their seasonal meridional shifts. There are a number of regions that are not similar. The OLR shows contributions of about 20%–30% in the southeast subtropical Pacific and Atlantic and in the northeast subtropical Pacific. The variance in these regions is again considered to reflect changes in SST, moisture, and nonconvective cloud cover, and therefore, does not show up in the HRC. Similarly, over the

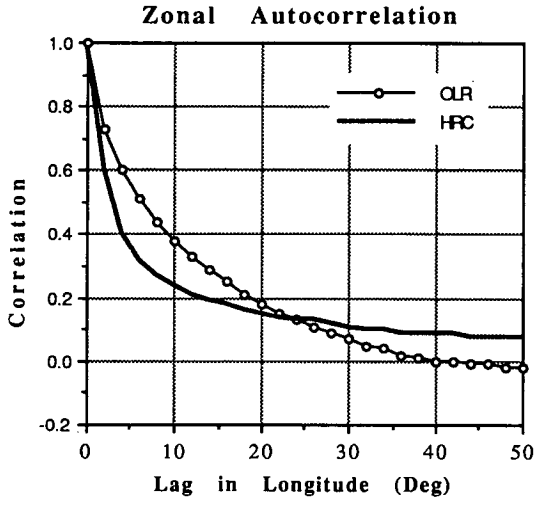

FIG. 4. Zonal autocorrelations for HRC (thick) and OLR (circles). Autocorrelations were computed for each zonal strip in the region 10°N–10°S from 60°E to 180° for each time period (pentad) and then ensemble averaged. In all cases of correlation shown in the plots, the number of products in the correlation exceeds 300 000.

TABLE 1. Time scale classification.

Time scale (days)	Denotation
512–2560	interannual
284–426	annual
66–256	semiannual
25–65	30–60 day
10–24	high frequency

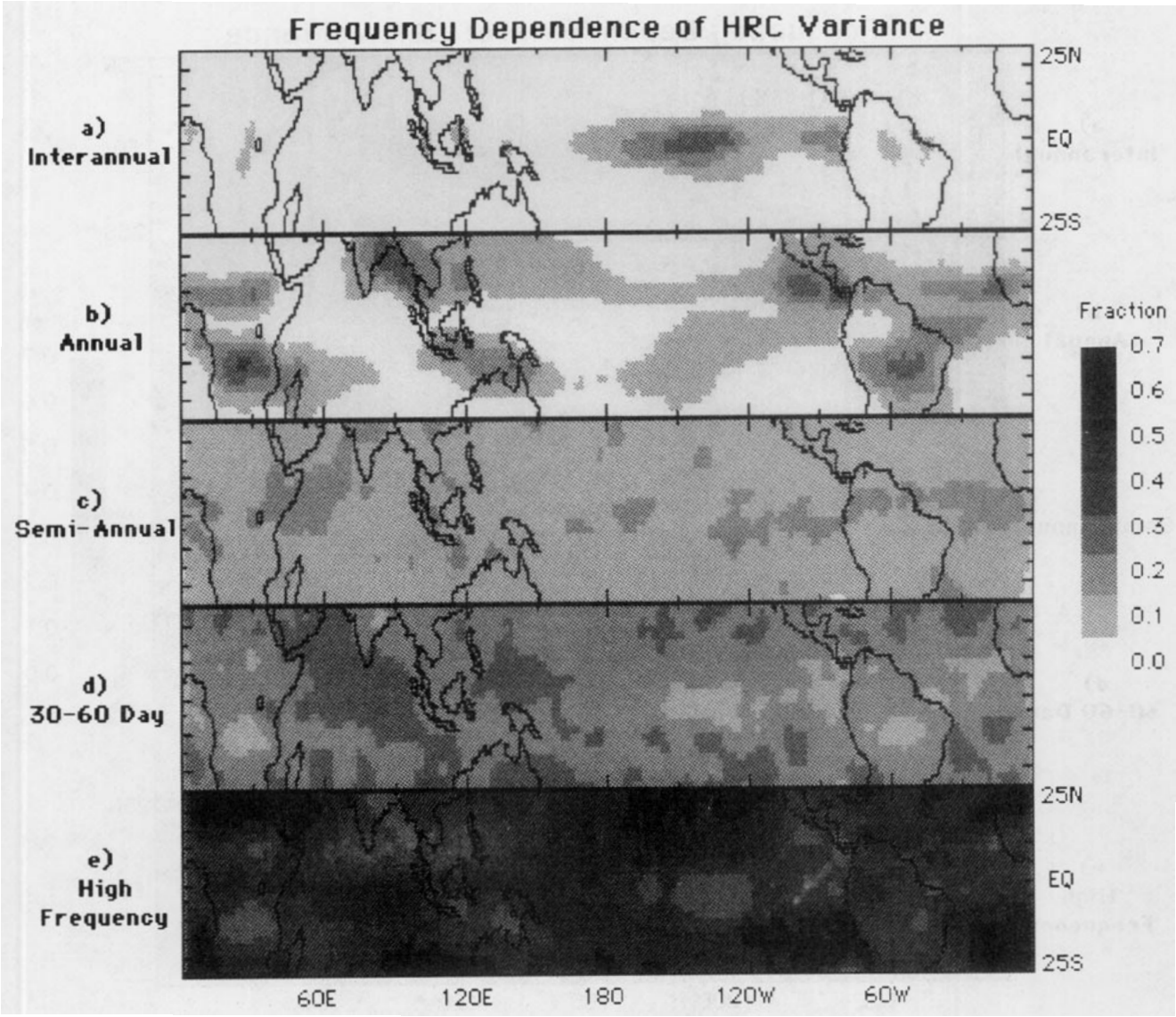

FIG. 5. The fractions of total HRC variance in the following frequency bands: (a) interannual, (b) annual, (c) semiannual, (d) 30–60 day, and (e) high frequency. See section 2e, section 4b, and Table 1 for details.

Sahara desert, the large annual signal in the OLR data is due largely to the variability in surface temperature, not to deep tropical convection.

At semiannual time scales (Fig. 5c and 6c), the HRC and OLR maps show very different spatial structures. The HRC shows contributions of about 20% mostly near the equator, while the OLR shows maximal contributions of about the same magnitude in many regions throughout the tropics. As mentioned in section 2e, the Fourier decomposition is not optimal to decompose all time scales. In particular, in regions where a strong annual cycle existed in the form of sharp peaks during one part of the year (e.g., just south of the equator in the eastern Pacific and in monsoon regions) it was found that part of the annual cycle signal was aliased to the semiannual time scale.

Figures 5d and 6d compare the contributions to the HRC and OLR variance from the 30–60 day time scale. The spatial structures for the HRC and OLR are very similar, each showing maximum contributions in the Indian Ocean and western Pacific Ocean with very little signal elsewhere: for example, eastern Pacific or Atlantic oceans. This spatial structure is in agreement with the "intraseasonal" OLR variance given in Lau and Chan (1988). The results here show that the 30–60-day signal for OLR contains a slightly greater fraction of the total variance than HRC in the regions that have substantial variability at this time scale. The OLR maxima are about 40%, while the HRC maxima are about 30%.

Last, the high-frequency variability for the HRC and OLR is compared in Figs. 5e and 6e. The OLR con-

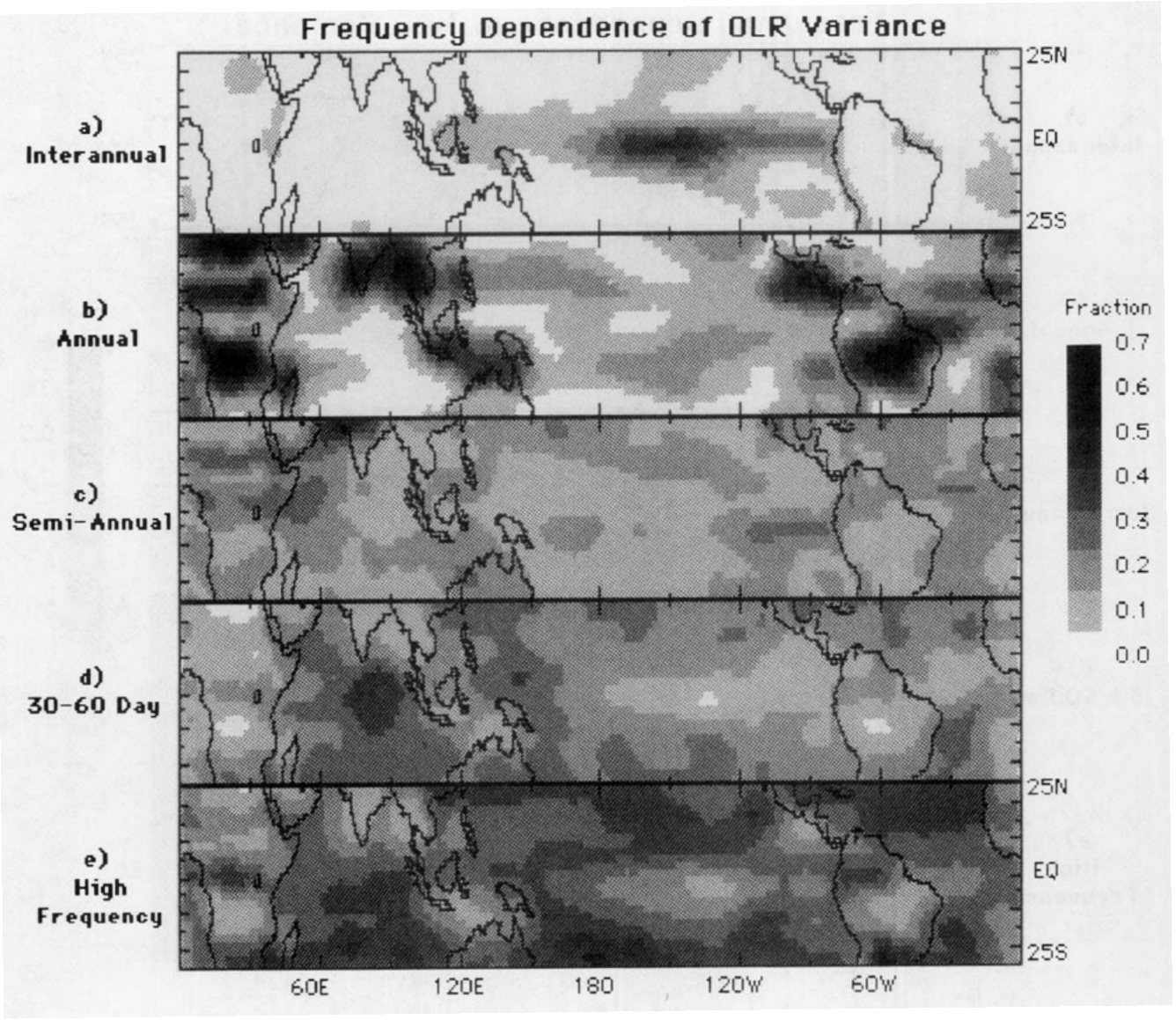

FIG. 6. Same as Fig. 5 but for OLR.

tributions are greatest in the convergence zones and in the near-subtropical areas, about 30%–40%. The HRC contains significantly greater contributions in the high-frequency band. These contributions are nearly 50% throughout the convergence zones. Even higher contributions exist in areas where deep convection is less frequently occurring (e.g., off the west coast of South America). In these regions, the HRC time series consist of only a few isolated events giving rise to a very white spectrum. For these cases, a large fraction of the variance occurs in the high-frequency band.

c. *Coherence*

To examine the frequency dependence of the correlation between the HRC and OLR, the coherence was computed for each point in the study domain (see section 2e). The coherence was averaged over the same five frequency bands described in Table 1, and the results are shown in Fig. 7. Confidence level estimates for the coherence values are given in Table 2. Not surprisingly, the coherence at interannual time scales (Fig. 7a) is highest ($\sim$0.9) over the central and eastern equatorial Pacific where the major convection anomalies associated with El Niño occur. Other regions of elevated interannual coherence appear over the equatorial Atlantic, near-equatorial South Indian Ocean, and the northern and southern tropical western Pacific. With respect to annual time scales (Fig. 7b), the coherence is high (0.7–0.9) where there is a strong annual cycle of convection in both datasets. The regions not marked by a strong annual cycle have a coherence between about 0.5 and 0.7. The coherence in the semi-annual (Fig. 7c) and 30–60-day bands (Fig. 7d) is

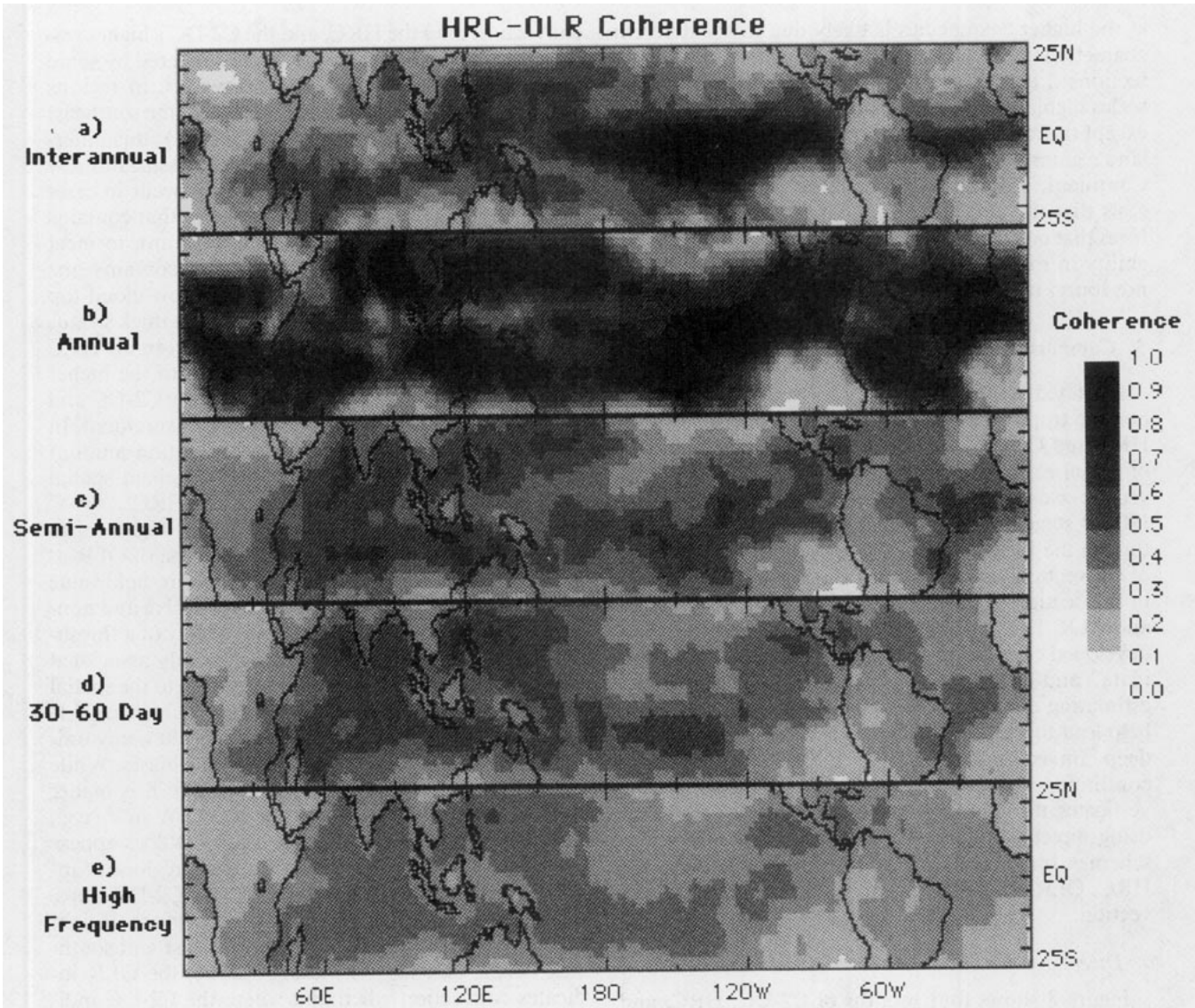

See section 2e and section 4c for details. Confidence level estimates are given in Table 2.

highest where there are highs in OLR and HRC variability at these time scales. For the semiannual time scale the highest values of coherence are about 0.6. For the 30–60-day band, the highest values of coherence are about 0.5 to 0.6. The coherence of the high-frequency variability (Fig. 7e) is typically between 0.3 and 0.4, being slightly lower in the convergence zones of the Pacific and Atlantic. The diminished coherence

TABLE 2. Confidence limits on coherence estimates. The table below gives the 95% lower confidence limit of the sample coherence-squared based on the number of degrees of freedom (ν) (Goodman, 1957). The degrees of freedom for the five frequency bands of Table 1 are interannual: 8, annual: 6, semiannual: 40, 30–60 day: 84, high frequency: 202.

	Sample coherence squared								
ν	0.10	0.20	0.30	0.40	0.50	0.60	0.70	0.80	0.90
8	0.026	0.040	0.064	0.103	0.167	0.259	0.386	0.550	0.754
49	0.018	0.064	0.134	0.221	0.322	0.436	0.561	0.697	0.843
80	0.029	0.093	0.175	0.269	0.372	0.484	0.603	0.729	0.862
200	0.047	0.126	0.217	0.315	0.418	0.527	0.640	0.756	0.877

at the higher frequencies is likely due to the different characteristics of the two measurements discussed in sections 2 and 3 and the difference in decorrelation scales highlighted in section 4a and Fig. 4. In all bands except the interannual, the coherence is lower over the land regions, including the large islands of the Maritime Continent. The diminished coherence over land suggests that the stronger variations in surface temperatures that occur over land are producing spurious variability in the OLR with regards to convection that is not found in the HRC.

5. Comparisons and validation using ISCCP C2 data

As stated earlier, the most climatologically comprehensive tropical convection (satellite) datasets are the HRC and OLR. However, the most detailed analysis of global cloud properties/types, including deep convective clouds, is contained in the shorter-record, ISCCP stage C2 dataset discussed in section 2c. Although the ISCCP C2 dataset (or any remote measure of convection) is not without shortcomings, it is used in this section as "truth" to further compare the HRC and OLR. The purpose here is to utilize a more recently developed convection index to help qualitatively "validate" and assess the use of the HRC and OLR for estimating deep tropical convection. Further, it may help lead to the construction of a longer time series of deep convection starting with the HRC or OLR and continuing with the ISCCP C2 data. This section investigates the relationships between these three data using direct comparisons, correlations, and applying schemes intended to determine how consistent the HRC, OLR, and C2-DC are in identifying deep convection.

a. Direct comparisons

Figure 8 shows four months of C2-DC, HRC, and OLR data during 1984. This figure is provided to show the typical values associated with the three convection indices. The OLR is scaled so that only regions having OLR values less than 260 W m^{-2} are assigned values. The value of 260 W m^{-2} was chosen so that essentially the same spatial area for each of the three datasets was covered by "indications" of deep convective clouds.

Comparing first the C2-DC data to the HRC, there are two general differences: the C2-DC has more area covered by nonzero amounts of deep convection than the HRC, and the HRC is not as smooth as the C2-DC. The contrast in areas covered by nonzero amounts of convection is believed to be partially due to the higher temporal sampling rate of the C2-DC but more importantly due to the difference in spatial scales used to define deep convection. The HRC defines a convective event only if its size is on the order 200 km or larger. The C2-DC, however, will define a convective event if its size is on the order 5–10 km. Thus, the C2-DC is measuring/identifying a much smaller scale of convection than the HRC, and the C2-DC's higher resolution of sampling yields more area covered by some indication of deep convection. However, in regions typically free from deep convection (e.g., the southeast Pacific and Atlantic and northern Africa), this difference could indicate an occasional misclassification by the objective C2-DC criteria. This may occur in cases when viewing a multilayer cloud system that contains enough liquid water throughout the column to meet the high optical thickness criteria and contains one cloud layer high enough to satisfy the low cloud-top pressure criteria (e.g., a cirrus layer over a thick stratus layer). The difference in smoothness between the HRC and C2-DC fields is believed to be due to the higher temporal and spatial sampling rates of the C2-DC and possibly the subjectivity of the HRC measurement. In general, in the regions where the convection amount exceeds 10% for the C2-DC there is excellent spatial agreement between the C2-DC and the HRC.

In comparing the C2-DC to the OLR, Fig. 8 raises three important issues in regard to the use of OLR as an indicator of tropical convection: 1) a threshold value is required to distinguish between convective and nonconvective regions, 2) due to the necessity of a threshold, anomalies in OLR are not necessarily associated with anomalies in convection, and 3) due to the spatial inhomogeneity of the parameters that influence OLR (e.g., SSTs, water vapor, tropopause height), any uniform threshold will be subject to regional biases. While the threshold of 260 W m^{-2} used in Fig. 8 is higher than the more often used value of 240 W m^{-2} (e.g., Lau and Chan 1983; Morrissey 1986), it does appear mostly successful in capturing the same regions of intense convection that are indicated by the C2-DC maps. However, it has mixed success in the regions of light convection. For example, in the northeast and southeast Pacific and the northeast Atlantic, the OLR indicates convection when and where the C2-DC indicates convection more consistently than the HRC. On the other hand, there are regions where the OLR does not quite encompass the full areas of convection indicated by the C2-DC and HRC, such as those at the fringes of the convection zones, and over the African continent. These issues of OLR thresholds and consistency between convection indices are examined further in section 5c.

b. Correlations

In this section, the correlations between the C2-DC dataset and the HRC and OLR datasets are examined. In addition, since OLR is an integrated measure that includes radiative effects from the surface, boundary-layer conditions, and all cloud types, its variations are attributable to more processes than the deep convection process alone. Therefore, correlations of some nonconvective fields/processes with the HRC and OLR data are also compared to these same correlations computed with the C2-DC data to show the degree to

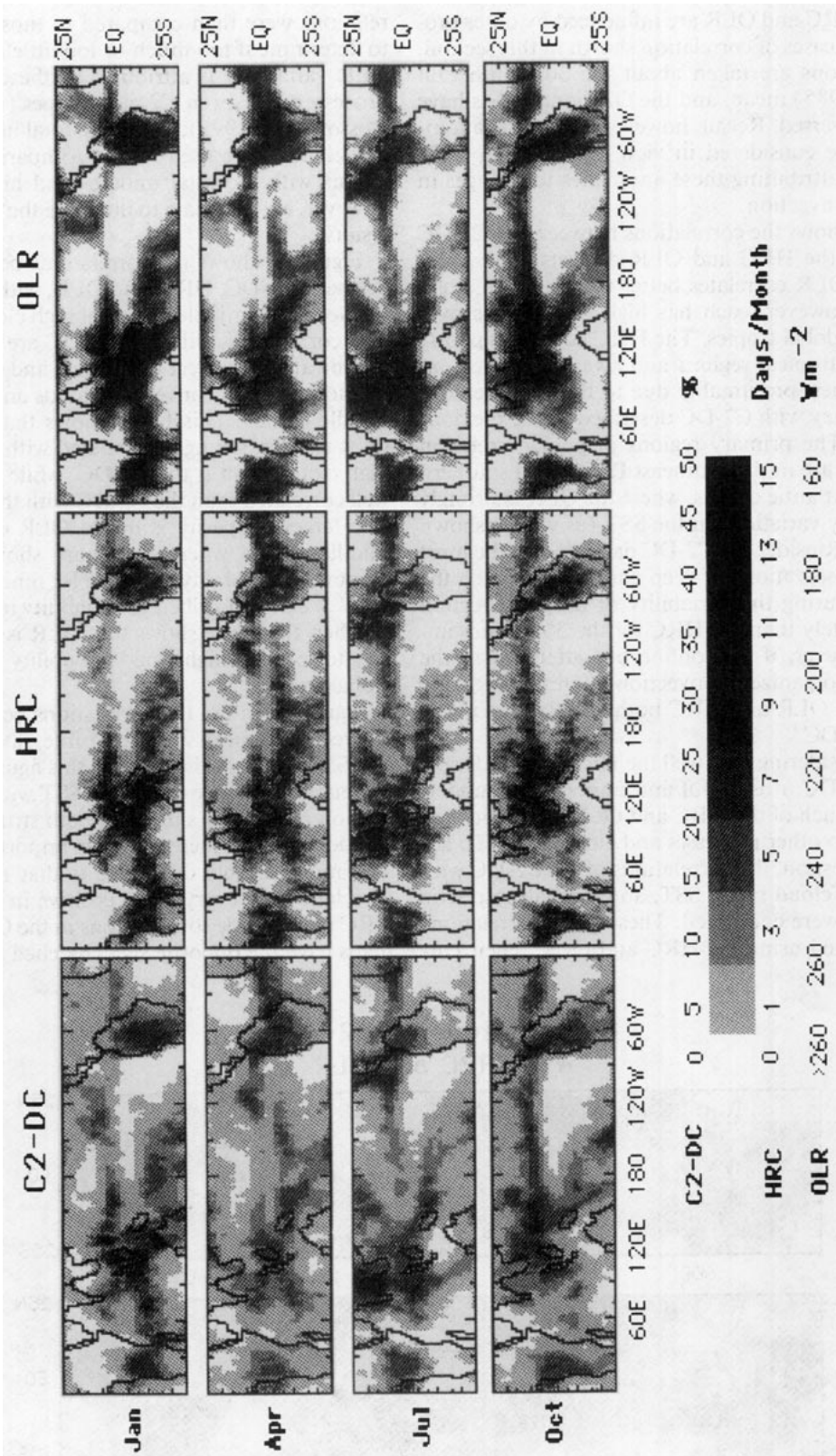

FIG. 8. Comparison of monthly mean maps of C2-DC (left), HRC (middle), and OLR (right) for January, April, July, and October of 1984. Gray scale at bottom provides the values for all three indices. All OLR values greater than 260 W m^{-2} are white.

which the HRC and OLR are influenced by other processes. In all cases of correlation shown in this section, the correlations are taken about the 30-month (Jul 1983–Dec 1985) mean, and the OLR anomalies have their sign reversed. Recall, however, that OLR anomalies must be considered in view of the mean OLR value when attributing these anomalies to changes in organized convection.

Figure 9 shows the correlations between the C2-DC dataset and the HRC and OLR datasets. The figure shows that OLR correlates better to the C2-DC than the HRC; however, each has high correlations over most of the global tropics. The HRC correlates poorly near the subtropical regions and away from the convergence zones, presumably due to the same reasons for discrepancy with C2-DC described in the previous subsection. The primary regions of poor correlation for the OLR are in the southeast Pacific and southern Indian and Atlantic oceans, where the OLR is strongly influenced by variations in the SST (as will be shown later). If we consider the C2-DC dataset to be the most accurate "observations of deep convection," then the OLR is capturing the variability of deep convection more accurately than the HRC for the 30 months analyzed. However, if we confine our attention to the areas where organized convection is climatologically frequent, the OLR and HRC both correlate very well with the C2-DC.

When considering how well the HRC and OLR correlate to C2-DC, it is useful and important to understand how much of the HRC and OLR variability can be ascribed to other processes and cloud types. To address this question, the correlations of the C2-DC with the other C2 cloud types, SST, and total atmospheric water vapor were computed. These same correlations were computed using the HRC and OLR. Their correlations were then compared to those of the C2-DC to determine if too much or too little of the HRC and OLR variability is attributed to these nonconvective processes. All seven C2 cloud types (see appendix C, Rossow et al. 1991), including total high, middle, and low clouds were used in this comparison. The correlations with the total middle- and high-level clouds, however, are adequate to illustrate the most important results.

Figure 10 shows the correlations between the three datasets, C2-DC, HRC, and OLR, with the (ISCCP C2 defined) total middle and total high cloud frequencies. The correlations with the C2-DC are used as a guide to indicate the correct magnitude and structure of correlation between convective clouds and total high and middle clouds. This figure shows that in general the OLR is more strongly correlated with the middle and high clouds than is the C2-DC, while the HRC is less well correlated than the C2-DC with these cloud types. The largest disparity is in the OLR correlation with middle clouds where the figure shows that a large amount of variability ($r > 0.75$ for much of the tropics) of OLR can be ascribed to variability in middle clouds. Further, the figure shows that OLR is an excellent estimator of total high cloud variability for much of the global tropics.

Figure 11 shows the correlations between the three convective indices with total integrated water vapor and SST. Overall, the maps in this figure show that the correlation of water vapor and SST with the three convection indices are similar in both structure and magnitude, although there are some important differences. The most notable difference is that the signs of the correlation are everywhere positive in the C2-DC and HRC maps, while some regions in the OLR correlation maps have the opposite sign (hatched regions). These

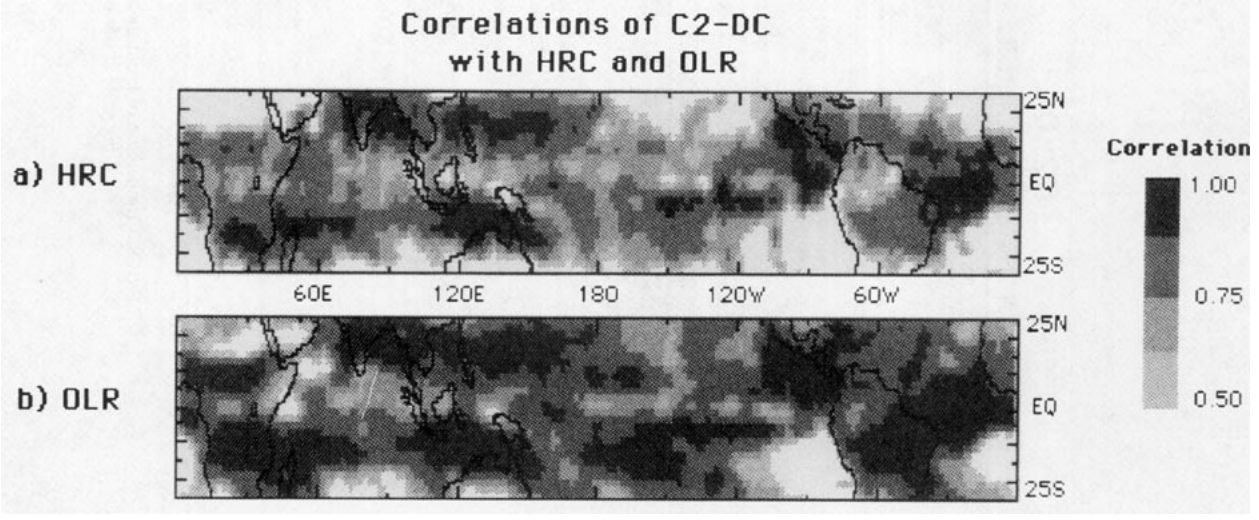

FIG. 9. Correlation maps of C2-DC with (a) HRC and (b) OLR. Correlations are computed using the 30 months of overlapping data about the 30-month means. The gray scale was chosen so that only values above 0.5 are delineated (0.5 gives the 99% confidence level for 30 measurements of two uncorrelated variables). OLR anomalies have their signs reversed.

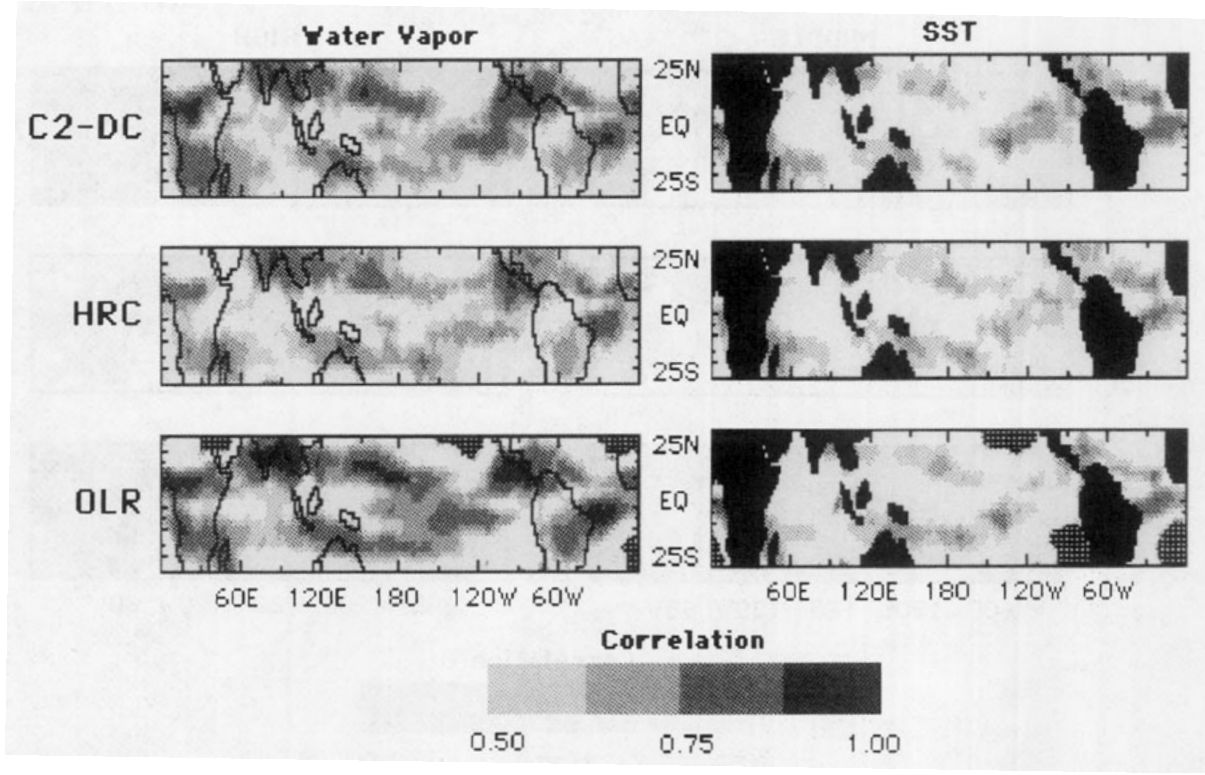

FIG. 10. Correlation maps among C2-DC (top), HRC (center), and OLR (bottom) with ISCCP-defined frequency of total middle (left) and total high (right) clouds. Correlations are computed using the 30 months of overlapping data about the 30-month means. The gray scale was chosen as in Fig. 9. OLR anomalies have their signs reversed.

occur in regions where convection is not climatologically persistent, and the OLR is more often subject to change associated with variations in SST that produce correlations of the opposite sign as those with respect to convection (remember OLR anomalies have their sign reversed, and low SST and intense convection imply low OLR). Another important difference is that the OLR field appears the most sensitive to the water vapor field. This elevated correlation is due to the strong dependence of OLR on the longwave emission from the water vapor in the atmosphere. In warm regions, increased amounts of water vapor lift the effective water vapor emitting level to higher (cooler) altitudes and therefore decrease the OLR value.

c. *Agreement in identifying deep convection*

If the C2-DC data can be taken as the best available satellite-derived index of deep convection in the tropics, the discussion in section 5a and the comparisons in Fig. 8 raise important issues regarding the identification of deep convection when using the HRC and OLR. The datasets differ in terms of their logistics and interpretation (e.g., units and necessity of threshold) and in their ability and/or accuracy at identifying regions undergoing deep convection. In this section, a measure of "agreement" is developed to help determine how well these three datasets agree at simply identifying deep convection. The results from this analysis will not address agreement in absolute amounts of convection (e.g., the HRC shows 10 days/month, and the C2-DC shows 33%); they are designed to show how well and where these datasets agree in categorically identifying regions undergoing deep convection.

The agreement between two convection indices at any point is calculated by mapping each convection index time series into a series of binary values, where a one (zero) indicates that convection did (did not) occur, based on a specified threshold value. Then, the two binary-valued time series are "correlated." The details of this calculation are given in the Appendix. The agreement measure (denoted **a**) ranges between 0 and 1, where 1 means that the two convection indices agreed completely on whether or not there was deep convection for the observations compared. A 0 means that the two convection indices disagreed completely on whether or not there was convection for the observations compared. If the agreement is 0.5, then the indices agreed for half the observations.

The average agreement (see the Appendix) for the

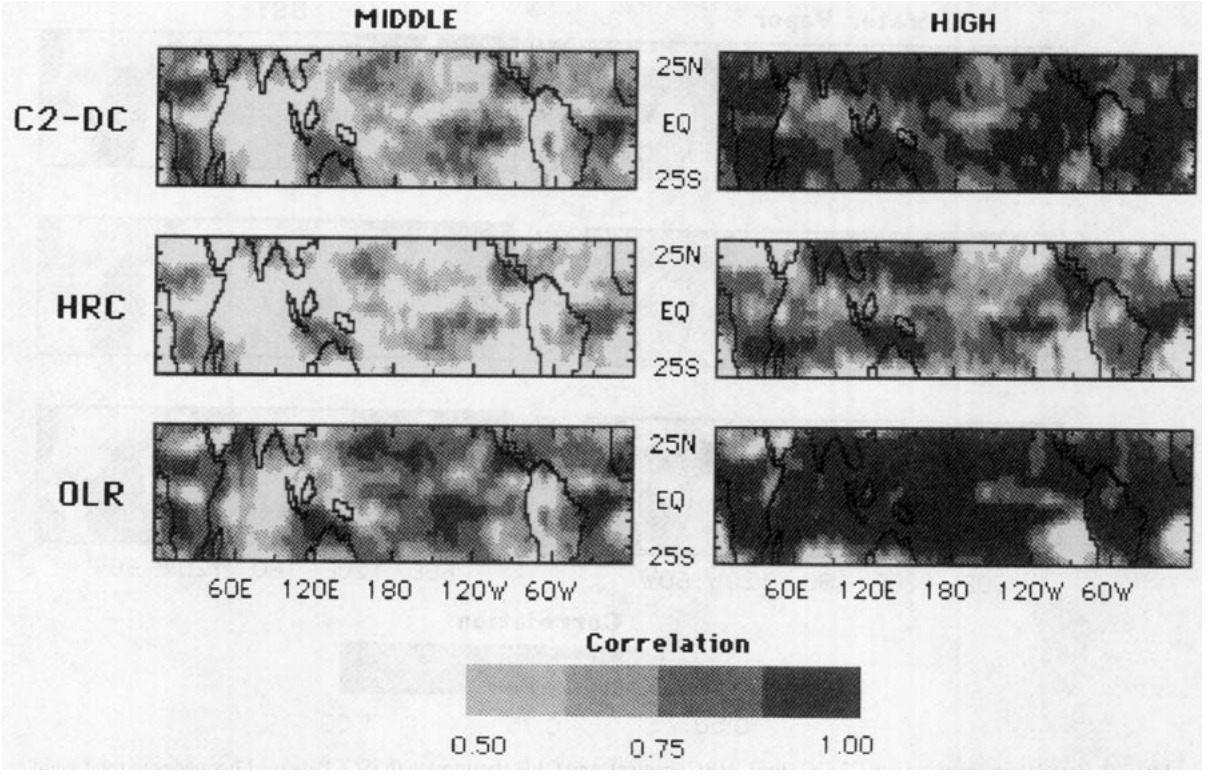

FIG. 11. Correlation maps among C2-DC (top), HRC (center), and OLR (bottom) with TOVS integrated water vapor (left) and SST (right). Correlations are computed using the 30 months of overlapping data about the 30-month means. The gray scale was chosen as in Fig. 9. Hatched areas are regions of negative correlation. OLR anomalies have their signs reversed.

entire tropical region was computed between each pair of convection indices as a function of the full range of possible thresholds (τ). The results of these computations are shown in Fig. 12. This figure shows that using high values of an OLR threshold is consistent with using low values of C2-DC and HRC thresholds, and vice versa. For example, it shows that an OLR threshold value of 240 W m^{-2} gives best overall agreement with a C2-DC threshold of about 5%, and a HRC threshold of about 2 days/month. The figure shows that using high values of a C2-DC threshold are consistent with using high values of an HRC threshold; likewise for low values. The results from this figure were used to select thresholds for the agreement calculations discussed in this section. These reference diagrams are useful when comparing values from different convection index datasets.

Two different types of thresholds were investigated. These thresholds were designed to address the agreement in distinguishing between 1) zero and nonzero amounts of deep convection (hereafter zero/nonzero amounts) and 2) zero-to-light and heavy amounts of deep convection (hereafter zero/heavy amounts). For testing the agreement in identifying zero/nonzero amounts of convection, the thresholds for C2-DC and HRC were set at 0% and 0.0 days/month, respectively (i.e., $\tau^c = 0\%$ and $\tau^h = 0$ days/month). The threshold for OLR was set (to the nearest 5 W m^{-2}) using the data in Fig. 12, and the constraint that the average agreement across the global tropical domain between it and the other index (HRC and C2-DC) was maximized. This led to an OLR threshold of 270 W m^{-2} for the comparison with C2-DC and 260 W m^{-2} for the comparison with HRC. For testing the agreement in identifying zero/heavy amounts of deep convection, the threshold for C2-DC was set at 10%. This threshold was chosen arbitrarily to filter out the "observations" of very light convection. The threshold for OLR was set in this case by maximizing the average agreement between C2-DC and OLR across the total tropical area. This gave a value of 230 W m^{-2}, a value that is consistent with the thresholds often used to distinguish convective from nonconvective regions. The threshold for HRC was set by maximizing its average agreement with C2-DC ($\tau^c = 10\%$) giving a threshold of 3.5 days/month.

Figure 13 shows the agreements between the three convection indices in identifying zero/nonzero

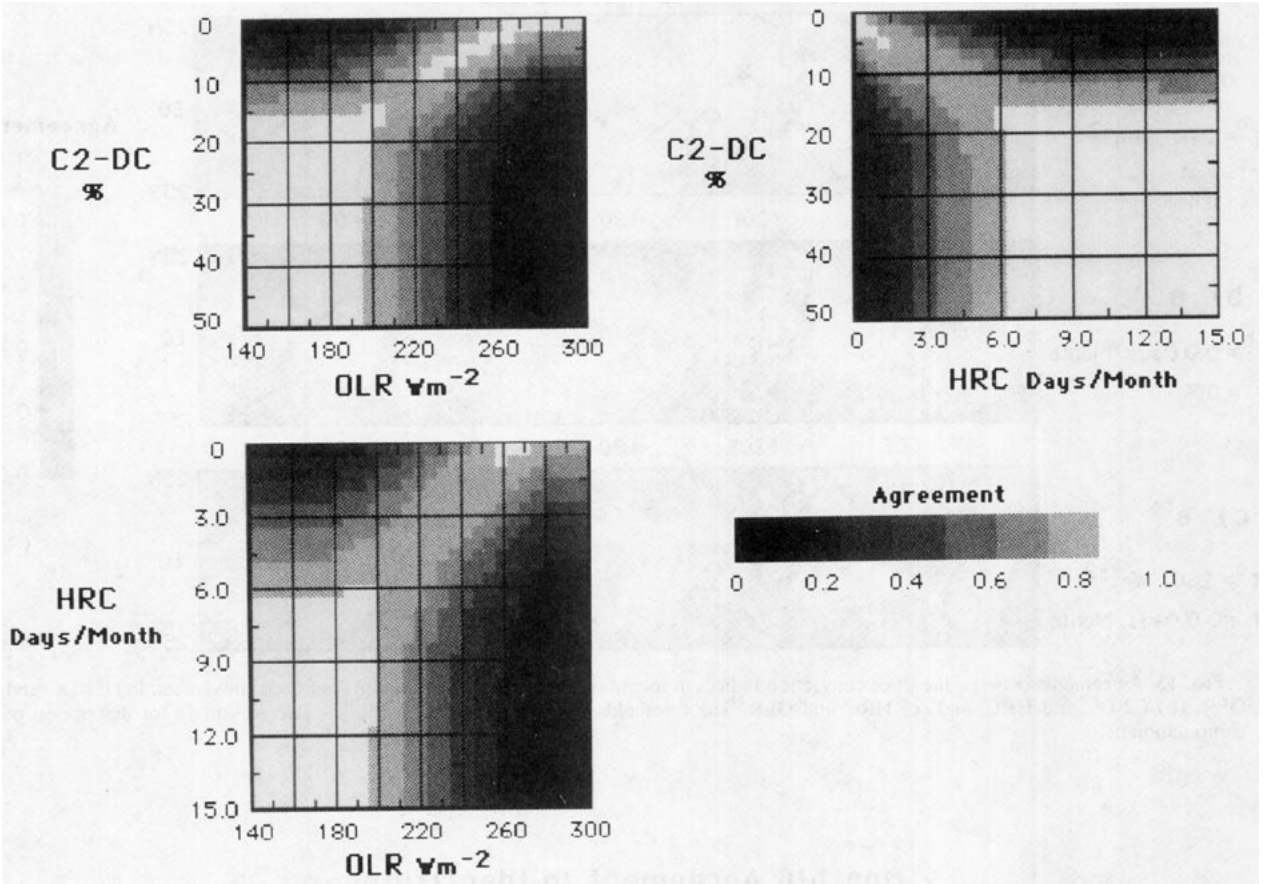

FIG. 12. Average agreements as a function of threshold values for the entire global tropical domain (see section 5c and the Appendix) among (a) C2-DC and OLR, (b) C2-DC and HRC, and (c) HRC and OLR.

amounts of convection. The figure shows that all of the indices are in good agreement (0.9–1.0) in the major convective zones and over the equatorial regions of the continents. The agreement diminishes away from these zones and in most cases is poorest near the subtropical regions. Overall, the areal extent of highest agreements (0.9–1.0) is greatest between C2-DC and OLR ($\mathbf{a}^{co}$), and least for HRC and OLR ($\mathbf{a}^{ho}$). Figures 13a and 13b show that both the HRC and OLR are in poor agreement with the C2-DC data over northern Africa, near Australia, and in the southern Atlantic. Additionally, the OLR is in poor agreement with the C2-DC in the southeast Pacific and at the eastern edge of the SPCZ, regions where the HRC agrees rather well with the C2-DC. On the other hand, the HRC is in poor agreement with the C2-DC in the northeast Pacific and Atlantic, regions where the OLR agrees rather well with the C2-DC. While the areal extent of highest agreement values is least for HRC and OLR, the areal extent of very poor agreement (<0.5) is also least. The results from this figure show that, on monthly time scales, all three convection indices are quite consistent at distinguishing convective from nonconvective conditions in the major zones of convection. Further, they show that discrepancies mostly arise at the edges of these zones, near the subtropics, and over some continental regions, where deep convection is less frequent.

Figure 14 shows the agreements between the three convection indices at identifying zero/heavy amounts of deep convection. The goal in this case is to determine if and where large errors in convection identification occur; that is, how often one index indicates intense convection for a particular region, while another indicates little or no convection. Contrary to the previous figure, the regions away from the major zones of convection (ITCZ, SPCZ, etc.) show very good agreement. On the other hand, the major zones of convection have the poorest agreement. The agreement values are, however, still relatively high (>0.7) in these regions. The fact that the agreement is least in these convectively intense regions is simply due to both convection indices not always being over/under the given thresholds for each month. For example, the thresholds for $\mathbf{a}^{ch}$ are τ^c = 10% and τ^h = 3.5 days/month; for some months

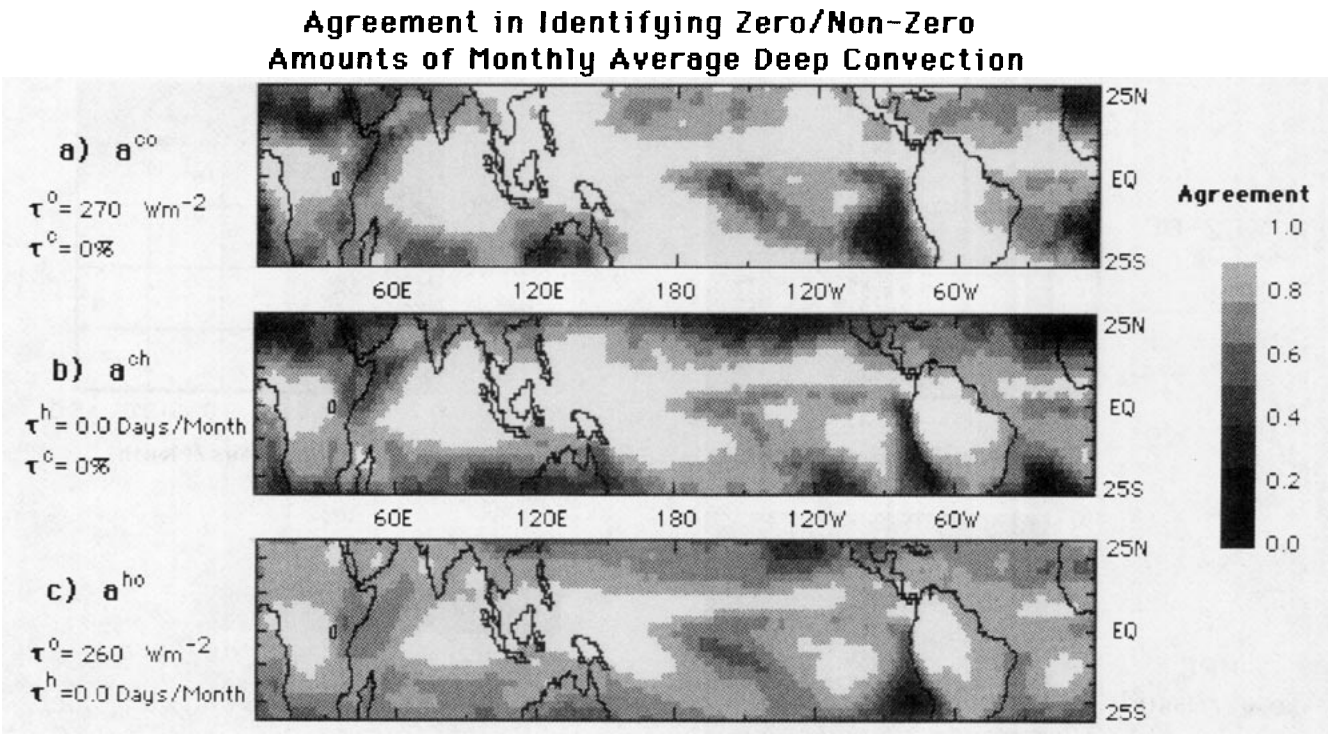

FIG. 13. Agreements between the three convection indices in identifying zero/nonzero "amounts" of deep convection. (a) C2-DC and OLR, (b) C2-DC and HRC, and (c) HRC and OLR. The thresholds used are specified on the left (see section 5c for description of computation).

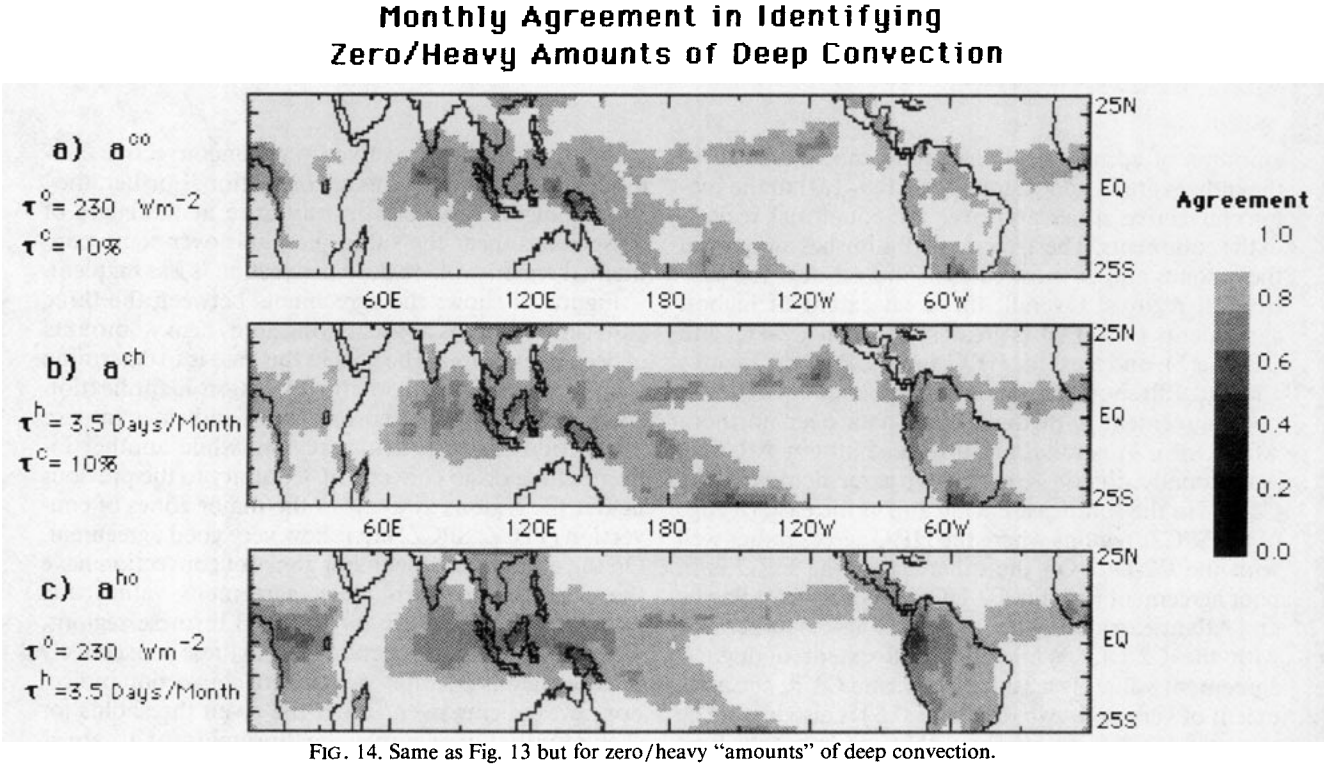

FIG. 14. Same as Fig. 13 but for zero/heavy "amounts" of deep convection.

the C2-DC will be just over its threshold, while the HRC will be just under. The results from this figure imply that when any of the convection indices are used conservatively (i.e., to identify very intense convection on a monthly time scale) over the tropical region, it is unlikely that any of them will make serious errors qualitative errors.

d. Biases in identifying deep convection

In this section, we explore the reasons for the inconsistencies between the three indices of convection revealed in the last section. To do this we develop a measure of bias, a complementary measure to the agreement construction. This bias calculation will determine if the disagreements shown in Figs. 13 and 14 are due to one of the variables consistently over/under identifying convection. From this information, it may be possible to draw some conclusions about which index may be more accurate and why for a given region.

The bias is calculated in a manner similar to the agreement; the details are provided in the Appendix. The bias measure (denoted **b**) ranges between -1 and $+1$, where a 1 means that the first index always identifies the location as convective and the second index always identifies the region as nonconvective (for the given thresholds τ). A value of -1 implies the opposite condition. A value of 0 implies that, for whatever number of disagreements there are, they cancel each other out, leaving no net bias. In these calculations, the same thresholds that were used for testing agreement in identifying zero/nonzero and zero/heavy amounts of deep convection are used here to investigate their biases.

Figure 15 shows the bias calculations for identifying zero/nonzero amounts of convection. The areas of large bias between the OLR and C2-DC ($\mathbf{b}^{co}$) are over northern Africa and Australia, where the OLR is indicating less convection than the C2-DC, and in the southeast Pacific and Atlantic, where the OLR is indicating significantly more convection than the C2-DC. The areas of significant bias between the HRC and the C2-DC ($\mathbf{b}^{ch}$) are the subtropical edges of nearly the entire tropical region, particularly northern Africa, the northeast Pacific, the southern Atlantic, over Australia, and off the western coast of South America. There is very little bias between the HRC and OLR ($\mathbf{b}^{ho}$); however, the figure again suggests that the OLR may be overestimating convection in the southeast Pacific and the HRC may be underestimating convection in the northeast Pacific. From the discussion in section 5a, it is clear that the reason the HRC underestimates convection in this context in the near-subtropical areas compared to the C2-DC is that the HRC identifies cluster-scale convection only, which is not as prevalent in the near-subtropical areas, while the C2-DC is able to identify small- to mesoscale ($\sim$5 km) convection features found in the near-subtropical regions. The

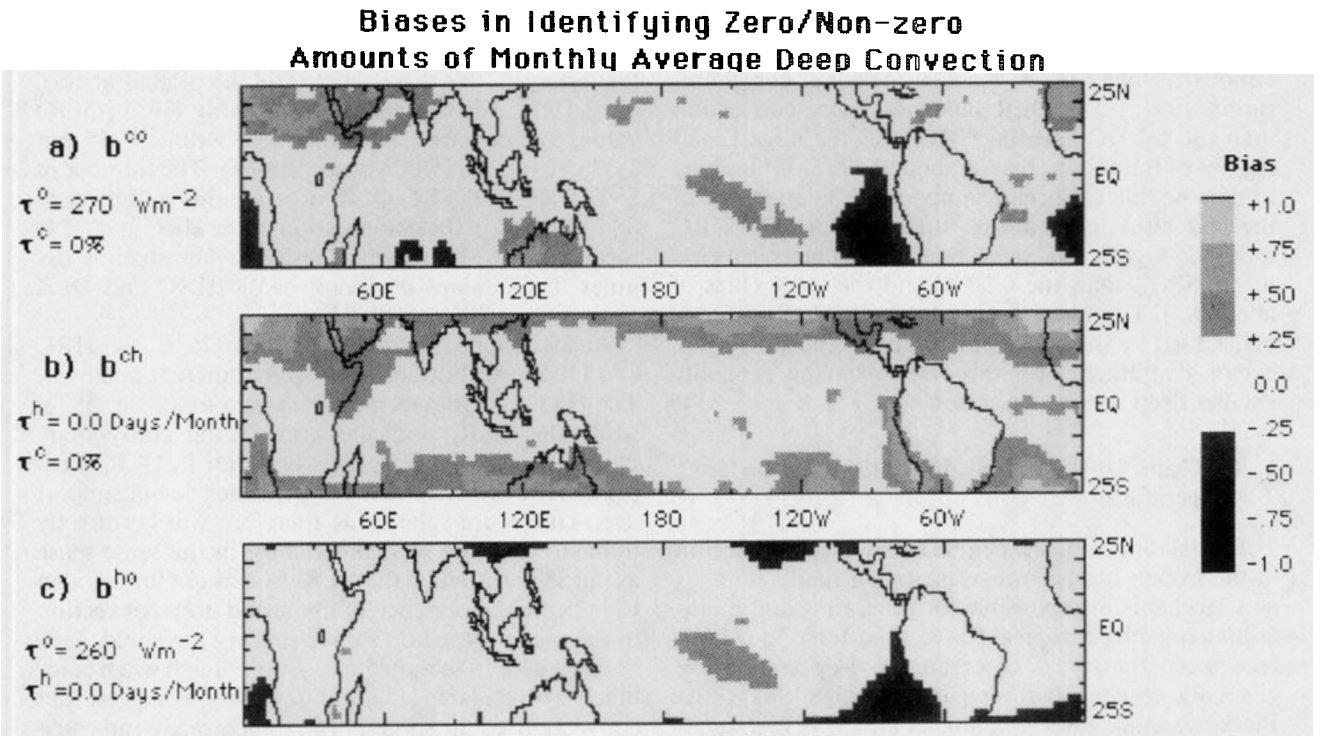

FIG. 15. Biases between the three convection indices in identifying zero/nonzero "amounts" of deep convection. (a) C2-DC and OLR, (b) C2-DC and HRC, and (c) HRC and OLR. The thresholds used are specified on the left (see section 5d for description of computation).

OLR is overestimating convection in the southeast Pacific and Atlantic due to the cool surface temperatures in these regions. These temperatures do not support deep convection, and the average OLR tends to be quite low, reflecting more directly the influence of the surface temperatures (see Fig. 11). Over northern Africa, the reasons for the OLR and HRC both underestimating convection is not as clear. Here, small-scale convection or rare occurrences of convection may be missed by the HRC, and may not have much impact on the average OLR, since the background surface temperatures are very high in this region.

The bias calculation for zero/heavy amounts of convection (not shown) showed large biases over the Andes Mountains and over the land regions in the western Pacific warm pool. Both the C2-DC and the OLR indicated more convection than the HRC over the Andes Mountains (bias of about 0.5), while the C2-DC and OLR were not biased in this region. Presumably, the OLR and C2-DC are indicating more convection over the Andes for different reasons. The OLR will be heavily influenced by the cold surface temperatures of the high-altitude terrain. The C2-DC indicates higher amounts of convection for possibly two reasons. First, as already noted, the C2-DC has a much higher spatial and temporal sampling rate, and therefore, it can observe smaller-scale convection and is less influenced by diurnal biasing. Second, since the Andes are snow covered, they will appear both bright in the visible and cold in the infrared, and therefore, may be incorrectly identified as indicating convection. This second reason, however, appears less likely since the algorithms were made very conservative for mountainous regions (W. B. Rossow, personal communication 1991). The OLR indicated more convection than the C2-DC and the HRC over the large island regions of Indonesia (bias of about 0.5). This bias may in part be due to surface temperature fluctuations of the high-altitude terrain on these islands. The HRC indicated slightly less convection at the subtropical edge of the SPCZ than the C2-DC and the OLR (bias of about 0.3). This bias is believed to be due to the smaller scales used by the C2-DC in defining deep convective events combined with this region having generally smaller deep convective scales.

6. HRC and OLR relationships to local sea surface temperature

The relationship between SST and deep convection in the tropics has been investigated in many contexts as a mechanism responsible for generating and maintaining organized tropical convection. It has long been recognized that areas of organized deep convection generally coincide with regions of high SST (e.g., Bjerkness et al. 1969; Manabe et al. 1974; Liebmann and Hartmann 1982). Many simple atmospheric models, which bear some resemblance to the real atmosphere, have been developed that parameterize atmospheric heating/convection on the basis of SST. Webster (1981) and Zebiak (1982, 1986) parameterized atmospheric heating anomalies using SST anomalies. Lindzen and Nigam (1987) parameterized low-level atmospheric forcing in terms of SST gradients. Neelin and Held (1987) parameterized atmospheric forcing (low-level convergence) using moist static energy that depends on absolute SST. Graham and Barnett (1987) and Zhang (1993) investigated the direct empirical relationship between OLR and SST on monthly and longer time scales, respectively. These latter two studies revealed that in the mean, over much of the tropical oceans, warm SST ($\gtrsim$27.5°) was a necessary but not sufficient condition for deep convection to occur (cf. Gadgil et al. 1984).

Because the relationship between SST and convection is so important and is not yet fully understood, it is vital that the proxies used for convection produce the same SST–convection relationships. This consistency will ensure that correct interpretations of the SST–convection relationship can be ascertained from observations. This section presents comparisons of the most basic convection-proxy and SST relationships. The comparisons are made on the basis of 2° × 2° monthly totals of SST, HRC, and OLR, from 1982 to 1987.

To compare the monthly HRC–SST and OLR–SST relationships, the mean HRC and OLR were computed as a function of local SST [similar to Graham and Barnett (1987), see their Fig. 5]. Figure 16 displays mean HRC (panel a) and OLR (panel b) values for 0.5°C SST bins for the entire tropical ocean region; for example, the mean HRC (OLR) plotted at SST = 29.5°C is the average of all monthly HRC (OLR) values that occurred over an SST between 29.25° and 29.75°C (about 15 000 observations). The number of SST–HRC and SST–OLR observations within each SST bin used in the computation of the HRC and OLR means is also shown (dark circles). The shading denotes the standard deviation of the HRC and OLR observations for each SST bin.

At temperatures between 14° and 26°C, the HRC and OLR distributions show quite different behavior. The HRC asymptotes rapidly to zero for cooler SSTs, while the OLR "indicates" increasing convection/clouds for cooler SSTs. This behavior in OLR is expected; the cooler surface temperatures do not support deep convection; the OLR therefore will be directly influenced by the SST and change in the same sense as the SST. Although the OLR value is not low enough to indicate the presence of organized deep convection in the mean (based on some arbitrary threshold, such as those used in section 5), it is low enough when combined with its large standard deviation to suggest that convection could sometimes be incorrectly indicated when SSTs are below 24°C. These relationships suggest OLR may be less reliable than HRC in representing

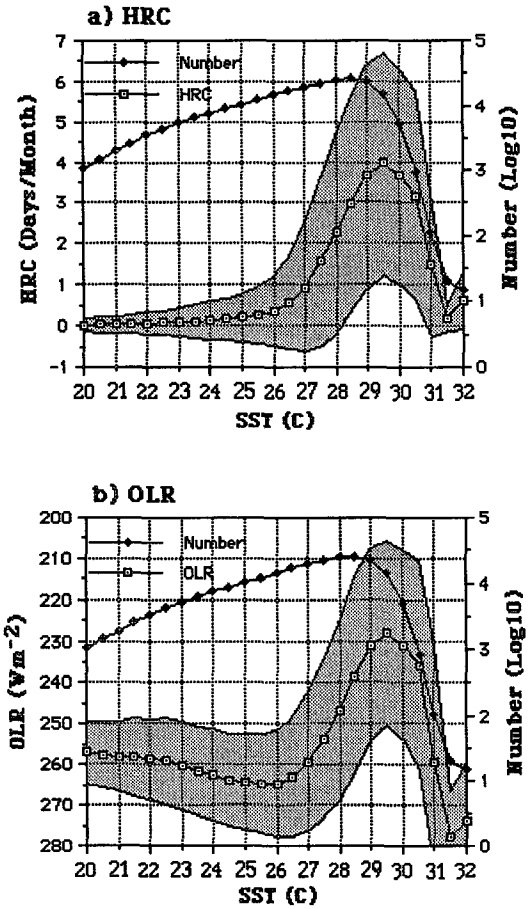

FIG. 16. Mean (a) HRC and (b) OLR values (left vertical axis) for 0.5°C SST bins. Values plotted are the mean HRC or OLR for all cases of a given SST value between 1982 and 1987 for the global tropical ocean regions. The number of observations (lines with dark circles) used in the computation of the means is specified on the right vertical axes. The standard deviation of the means are delineated by the shading. Statistical t tests at the 99% confidence level show that the mean values between 29.5° and 31.5°C are statistically different.

the relationship between SST and deep convection, or at least necessitates greater caution in interpretation when using OLR (See Figs. 11, 13, and 15).

For SSTs above 26°C, the behavior of HRC and OLR is nearly identical. Each plot implies a dramatic increase in convection in the SST range of 26.5° to 29.5°C. At higher temperatures, however, the implied convection decreases sharply to near zero over the warmest SSTs. This same calculation (not shown) was performed for the HRC in the western Pacific Ocean region, extending between 140°E and 150°W, and the diminished convection for higher SSTs (>29.5°C) is still apparent. Similar behavior can be seen in an analogous plot shown by Graham and Barnett (1987, see their Fig. 5). In their analysis the sample size precluded attaching statistical significance to this tendency for very high SSTs to be associated with decreased convection. In this study, however, the sample size is easily sufficient to statistically support this relationship (i.e., t tests at the 99% confidence level indicate that the mean values are statistically different for SST between 29.5° and 31.5°C). Adding to the confidence of this result is the fact that both the HRC and the OLR give nearly identical results. Although the regime where "convection" is an increasing function of SST (i.e., SST < 29.5°C) is well known and receives much attention, we briefly focus our attention in the discussion below on the regime where convection is a decreasing function of SST (i.e., SST > 29.5°C).

The preceding finding is important since it suggests that the maximum convective activity does not occur over the *warmest* (>29.5°C) water but rather the warmest water occurs under "clear," less convective skies. Physically, the result suggests that in general SSTs in excess of about 30°C occur only under conditions of diminished convection (e.g., large-scale subsidence). This reasoning is further supported in computations of the mean HRC anomaly as a function of both local absolute SST and local anomalous SST (not shown). These computations show that negative HRC anomalies (i.e., decreased convection) are associated with positive SST anomalies at absolute SST values in excess of 29.5°C. Additionally, the plots in Figs. 16a and 16b empirically demonstrate that in a highly convective regime the maximum equilibrium SST that can be supported is about 29.5°C. This value is near the low-end value calculated by Ramanathan and Collins (1991). Related computations by Newell (1979) and Graham and Barnett (1987) suggest values of about 30° and 28°C for clear and cloudy conditions, respectively. Further, since SSTs greater than 29.5°C tend to be observed only in regions (or times) of diminished convection; the plots are additional evidence that convective-cloud complexes provide a systematic and climatologically important cooling effect on the surface temperature (e.g., Somerville and Remer 1984; Ramanathan and Collins 1991). Finally, the facts (a) SSTs in excess of 29.5°C are not uncommon in individual (monthly) observations and (b) climatological average tropical ocean SSTs in excess of that value are rare indicate that very warm SSTs are unstable and drive the system toward the convective regime (e.g., Chertok et al. 1991; Ramanathan and Collins 1991; Zhang 1993). These results and ideas are discussed and analyzed in more detail in Waliser and Graham (1992).

To investigate the regional reliability and/or consistency of the SST–convection relationship shown in Fig. 16, the same calculations were done for five climatologically different tropical ocean regions. Figures 17a and 17b show the HRC–SST and OLR–SST relationships, respectively, for the 1) north Indian Ocean, 2) western Pacific, 3) eastern Pacific ITCZ, 4) eastern equatorial Pacific, and 5) Atlantic ITCZ regions. The error bars denote the standard error of the mean (only points with greater than 200 observations are plotted).

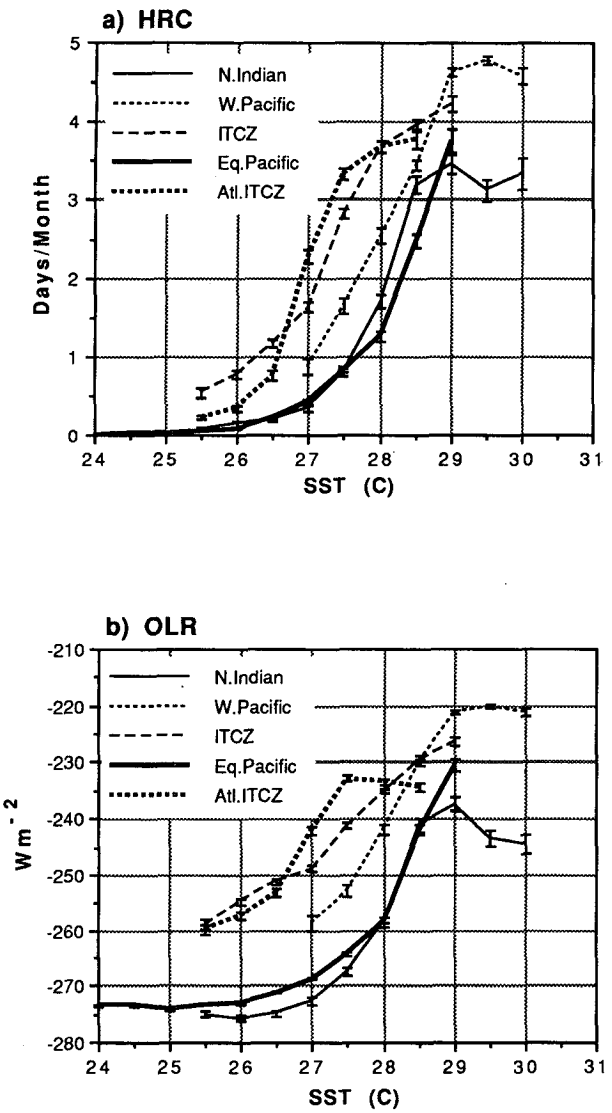

FIG. 17. Mean (a) HRC and (b) OLR values for 0.5°C SST bins. Values plotted are the mean HRC or OLR for all cases of a given SST value between 1982 and 1987 for the following five selected regions: 1) north Indian Ocean, 60°–105°E and 10°–25°N; 2) western Pacific, 120°–150°E and 10°S–10°N; 3) eastern Pacific ITCZ, 100°–140°W and 4°–12°N; 4) eastern equatorial Pacific, 100°–140°W and 10°S–4°N; and 5) Atlantic ITCZ 15°–45°W and 4°–12°N. Means are only plotted when 200 observations or more were available for the given SST bin. Error bars denote standard error of the means for each SST bin.

The HRC plots in Fig. 17a are all similar, each showing a near-zero convection response at low SSTs, a sharp rise at temperatures between 27° and 28°C (i.e., "threshold" temperatures), and in some cases a mild decrease of implied convection at the highest SSTs. The OLR plots in Fig. 17b show the same range of threshold SSTs in nearly the same order as the HRC, but the relationship of OLR to SST has greater regional dependence. For example, the regions denoted *N. Indian* and *Eq. Pacific* have much higher mean OLR values for almost the entire SST range. These regions are largely free of convection except during the Asian summer monsoons for the *N. Indian* region and during the boreal springs or warm phase of the ENSO cycle for the *Eq. Pacific* region. Therefore, an average of OLR over such areas will raise the OLR mean relative to nearby convectively active regions. These results further illustrate the problematic nature of using OLR as a convection proxy, especially in investigations of the relationship between SST (or moisture) and deep convection, or for cases where the study domain encompasses varying climatic regimes.

7. Summary and conclusions

This paper compares two long-term satellite-derived datasets used to study climatological aspects of organized tropical convection, the HRC and the OLR. The goal was to quantify the differences between these two datasets so that subsequent investigations requiring use of long-record convection proxy data would have at least the rudiments of a benchmark comparison to address the strengths and weaknesses of the dataset chosen and to determine what these imply for the end results of the investigation. The results of this study show important differences between the HRC and OLR when used for estimating large-scale deep convection. These include differences in the scales and variability of the estimated fields of convection, in their relationships to other tropical fields, and in the logistics of their use. A few of the more important differences and results from this study are summarized.

- The variance in the HRC field is more tightly confined to the convergence zones and deep tropics. The variance in the OLR, on the other hand, is much smoother with larger spatial scales due to the influences of SST, water vapor, and stratus cloud types (e.g., cirrus) on OLR. This difference in spatial scale is further emphasized by the contrast in zonal decorrelation; for 5-day data, the decorrelation scale of the HRC is about 800 km, while that for the OLR is about 1400 km.
- There are marked differences between the frequency-dependent variability of HRC and OLR. In general, the HRC has a greater fraction of its variance at high frequencies (10–25 days), while the OLR has more variance in the intraseasonal to interannual time scales. The high frequencies are believed to dominate the HRC record because these data primarily resolve convective cloud complexes that have relatively small time and space scales. The OLR observations, on the other hand, are subject to the evolution and variations of all cloud types and boundary-layer processes producing smoother time series with broader spatial scales. This aspect of OLR, in contrast to the HRC, leads to variability in regions not generally associated with deep convection.

• Direct comparisons of monthly HRC and ISCCP C2 convective data (C2-DC) showed that the C2-DC data contain more areas of nonzero amounts of convection and are smoother. The first difference is believed to be principally due to the difference in spatial scales used to define deep convection and also due to the greater sampling rate of the C2-DC. The HRC will define a convective event if its size is on the order 200 km or larger, while the C2-DC will define a convective event if its size is on the order 5–10 km. Therefore, the HRC captures cluster-scale events only while the C2-DC measures/identifies mesoscale and smaller convective events. Thus, the HRC frequently misses areas undergoing "light" or small-scale convection. The difference in smoothness is most likely due to the higher temporal and spatial sampling rates of the C2-DC.

• Direct comparisons of monthly OLR to C2-DC (or HRC) raise three important issues in regard to the use of OLR as an indicator of tropical convection: 1) a threshold must be applied to distinguish between convective and nonconvective conditions; 2) anomalies in OLR can be attributable only to anomalies in convection when the absolute OLR values are near this threshold; and 3) due to the inhomogeneity of the global tropical regions (e.g., SSTs, water vapor, tropopause height), any uniform threshold will produce regional biases in the estimated convection field.

• Correlation analysis showed OLR variations to be more strongly correlated to fluctuations of middle and high clouds (cirrus, cirrostratus and deep convective) than either HRC or C2-DC. In addition, OLR was found to be more strongly correlated to fluctuations in total integrated water vapor amount than either the HRC or C2-DC.

• An "agreement" analysis showed that in regions away from the major convergence zones there is poor agreement between the three indices in identifying light amounts of convection. On the other hand, the three convective indices agreed quite well at identifying intense/frequent amounts of convection in almost all regions of the tropics. A "bias" analysis demonstrated that the HRC indicates too little convection at the subtropical edges of the study domain, while the OLR indicates too much "convection" over the cold current areas, such as the Benguela and Peru currents, and over the large island regions of the Maritime Continent.

• A key component in this study was the comparison of the OLR and HRC relationships to local SST. These results strongly suggest that the OLR is a less reliable convection index for use in studies regarding the relationship between SST (or water vapor) and deep convection. This component of the study also led to a new and important finding, both the OLR–SST and HRC–SST relationships suggest that the amount of convection diminishes for SSTs greater than 29.5°C. Thus, the maximum convective activity does not occur over the *warmest* (>29.5°C) water; rather, the warmest water occurs under less-convective skies.

The differences between the HRC and OLR as outlined appear to stem mostly from the fact that HRC was designed to measure deep convection only, while OLR was not. Although HRC is a subjective measurement, it does have the advantage that it filters out (to a large degree) thin cirrus and nonconvective clouds that are not associated with large-scale convective systems through the incorporation of visible data (cf. Fu et al. 1990). These clouds contaminate or at least modify the temporal and spatial structures of the OLR estimates of convection. Further, the HRC does not include the direct "contaminating" effects from atmospheric moisture and surface temperature variations to which OLR is subject. These variations can produce ambiguous or incorrect convection indices over clear areas. Of even more serious consideration is the necessity of implementing a threshold when using OLR to distinguish clear from convective regions.

Given that the ISCCP C2-DC as well as microwave-based methods (passive and active) are generally superior at identifying tropical deep convection and precipitation, they suffer at this time from the brevity of their records. Currently, the HRC and OLR are the only long-term satellite-based datasets for climatological studies of tropical convection/precipitation. Based on the results from this study, it is believed that the HRC is equally adept as the OLR, if not superior, at representing the characteristics of cloud cluster–scale tropical convection. This is especially true in cases where 1) the spatial scales or frequency-dependent variability of convection are important, 2) the relationships between deep convection and SST or water vapor are being considered, and 3) the domain of interest is large enough to contain spatial inhomogeneities, such as land–sea contrasts or inhomogeneous SST and moisture fields.

Finally, one major goal of this work was to produce some guidance for extending the more modern convection indices (e.g., ISCCP) backward using the OLR or HRC. For some studies, it may be necessary to take advantage of the long records of the HRC or OLR, but still be important to use the most robust dataset when available. Given that the HRC contains both visible and infrared information in a frequency-type unit and that it compares qualitatively well with the ISCCP C2-DC, one simple method for extending the C2-DC backward would be to convert the HRC frequency to a C2 frequency (e.g., 6 days/month ~ 20% ISCCP units). This remapping was done for the overlapping time periods, and the biases and rms errors were calculated at each point in the domain. The results (not shown) show that the HRC is biased high (on the order of 5%–10% in C2-DC units, about 10%–20% of the C2-DC signal) in the western Pacific near land regions and over the tropical continents. This bias is due to the HRC inadequately resolving the diurnal signal (see Garcia 1980; Fu et al. 1990), and thus, is dependent on the equatorial crossing times of the satellites used

to create the HRC. The HRC is biased low by about the same amount over the Andes and the very southern edge of the SPCZ due to the reasons discussed in section 5d, and is biased low to a lesser degree away from the major convection zones for these same reasons. The rms errors over most of the tropical regions were on the order of 25% or less of the C2-DC signal. Beyond this simple approach, account would have to be taken of the regional differences between the two products, and regression or other methods would need to be undertaken.

Acknowledgments. The authors would like to acknowledge Oswaldo Garcia's contribution of creating the HRC dataset and to thank him for supplying us with the HRC data and providing helpful suggestions regarding the dataset and this study. We would like to thank John Horel for supplying us with the OLR dataset used in this study and William Rossow for helpful information regarding the ISCCP dataset. We would also like to acknowledge the constructive comments and suggestions from two anonymous reviewers. This research was supported by the NASA Graduate Research Fellowship Program under Grant NGT-50304 (DW), the California Space Institute under Mini-grants CS-88-89 and CS-45-90 (CG-DW), by NOAA Grant NA86AA-DCP104 for the Experimental Climate Forecast Center at the Scripps Institution of Oceanography (NG), and by NASA/WETNET Grant NAGW-2460 (CG). In addition, a large portion of the calculations were done on the Cray Y-MP at the San Diego Supercomputer Center (SDSC). SDSC was established with, and is principally supported by, grants from the National Science Foundation.

APPENDIX

Formalism for Convective Indices Comparisons

a. Computation of agreement

The measure of agreement (**a**) is computed as follows.

First, for each spatial location x, time index t, and convection index β, a binary-valued convection flag **c** is defined as

$$\mathbf{c}^{\beta}_{x,t} = 1 \quad \text{if} \quad \mathbf{v}^{\beta} > \tau^{\beta}$$

$$\mathbf{c}^{\beta}_{x,t} = 0 \quad \text{if} \quad \mathbf{v}^{\beta} \leqslant \tau^{\beta},$$

where **v** is the convection index value, τ is the threshold value, and $\beta = o$, h, and c for OLR, HRC, and C2-DC, respectively. Note, inequalities are reversed for $\beta = o$. The agreement, **a**, between two convection indices, β and γ, at spatial location x is then given by

$$\mathbf{a}^{\beta\gamma}_{x} = \frac{1}{N} \sum_{t=1,N}^{N} \alpha^{\beta\gamma}_{x,t},$$

where

$$\alpha^{\beta\gamma}_{x,t} = 1 \quad \text{if} \quad \mathbf{c}^{\beta}_{x,t} = \mathbf{c}^{\gamma}_{x,t}$$

$$\alpha^{\beta\gamma}_{x,t} = 0 \quad \text{if} \quad \mathbf{c}^{\beta}_{x,t} \neq \mathbf{c}^{\gamma}_{x,t}.$$

The average agreement for the entire tropical region is given by

$$\bar{\mathbf{a}}^{\beta\gamma} = \frac{1}{M} \sum_{x=1,M}^{M} \mathbf{a}^{\beta\gamma}_{x}.$$

b. Computation of bias

The measure of agreement (**a**) is computed as follows.

Using the same binary-valued convection flags (**c**) defined above, the bias **b** between two convection indices, β and γ, at spatial location x, is given by

$$\mathbf{b}^{\beta\gamma}_{x} = \frac{1}{N} \sum_{k=1,N}^{N} \alpha^{\beta\gamma}_{x,t},$$

where

$$\alpha^{\beta\gamma}_{x,t} = 1 \quad \text{if} \quad \mathbf{c}^{\beta}_{x,t} = 1 \quad \text{and} \quad \mathbf{c}^{\gamma}_{x,t} = 0$$

$$\alpha^{\beta\gamma}_{x,t} = -1 \quad \text{if} \quad \mathbf{c}^{\beta}_{x,t} = 0 \quad \text{and} \quad \mathbf{c}^{\gamma}_{x,t} = 1.$$

REFERENCES

Aida, M., 1976: Scattering of solar radiation as a function of cloud dimensions and orientation. *J. Quant. Spectrosc. Radiat. Transfer,* **17,** 303–310.

Arkin, P. A., 1984: An examination of the Southern Oscillation in the upper tropospheric tropical and subtropical wind field. Ph.D. dissertation, University of Maryland, 240 pp.

——, and P. E. Ardanuy, 1990: Estimating climatic-scale precipitation from space: A review. *J. Climate,* **2,** 1229–1238.

Bendat, J. S., and A. G. Piersol, 1986: *Random Data.* Wiley, 120–129.

Bjerknes, J., L. J. Allison, E. R. Kreins, F. A. Godshall, and G. Warnecke, 1969: Satellite mapping of the Pacific tropical cloudiness. *Bull. Amer. Meteor. Soc.,* **50,** 313–322.

Chertock, B., R. Frouin, and R. C. J. Somerville, 1991: Global monitoring of net solar irradiance at the ocean surface: Climatological variability and the 1982–83 El Niño. *J. Climate,* **4,** 639–650.

Coakley, J. A., Jr., and R. Davies, 1984: The effect of cloud sides on reflected solar radiation as deduced from satellite observations. *J. Atmos. Sci.,* **43,** 1025–1035.

Davies, R., 1984: Reflected solar radiances from broken cloud scenes and the interpretation of measurements. *J. Geophys. Res.,* **89,** 1259–1266.

Fouquart, Y., 1985: Radiation in boundary layer clouds. Report of the JSC/CAS Workshop on Modeling of Cloud Topped Boundary Layer, Fort Collins, CO, Report WCP 105, World Meteorological Organization, Geneva.

Fu, R., A. D. Del Genio, and W. B. Rossow, 1990: Behavior of deep convective clouds in the tropical Pacific deduced from ISCCP radiances. *J. Climate,* **3,** 1129–1152.

Gadgil, S., P. V. Joseph, and N. V. Joshi, 1984: Ocean–atmosphere coupling over monsoon regions. *Nature,* **312,** 141–143.

Garcia, O., 1981: A comparison of two satellite rainfall estimates for GATE. *J. Appl. Meteor.,* **20,** 430–438.

——, 1985: Atlas of Highly Reflective Clouds for the Global Tropics: 1971–1983. U. S. Department of Commerce, NOAA, Environmental Research Laboratory.

Gill, A. E., and E. M. Rasmusson, 1983: The 1982–83 climate anomaly in the equatorial Pacific. *Nature,* **305,** 229–234.

Goodman, N. R., 1957: On the joint estimation of the spectra, cospectrum and quadratic spectrum of a two-dimensional stationary Gaussian process. Ph.D. dissertation, Princeton University.

Graham, N. E., and T. P. Barnett, 1987: Sea surface temperature, surface wind divergence, and convection over tropical oceans. *Science,* **238,** 657–659.

Gruber, A., and A. F. Krueger, 1984: The status of the NOAA Outgoing Longwave Radiation Data Set. *Bull. Amer. Meteor. Soc.,* **65,** 958–962.

Gutzler, D. S., and T. M. Wood, 1990: Structure of large-scale convection anomalies over tropical oceans. *J. Climate,* **3,** 483–496.

Harshvardhan, 1982: The effect of brokeness on cloud-climate sensitivity. *J. Atmos. Sci.,* **39,** 1853–1861.

Hastenrath, S., 1990: The relationship of highly reflective clouds to tropical climate anomalies. *J. Climate,* **3,** 353–365.

Horel, J., and A. G. Cornejo-Garrido, 1986: Convection along the coast of northern Peru during 1986: Spatial and temporal variation of clouds and rainfall. *Mon. Wea. Rev.,* **114,** 2091–2105.

——, A. N. Hahmann, and J. E. Geisler, 1989: An investigation of the annual cycle of convective activity over the tropical Americas. *J. Climate,* **2,** 1388–1403.

Houze, R. A., Jr., and A. K. Betts, 1981: Convection in GATE. *Rev. Geophys.,* **19,** 541–576.

Kilonsky, B. J., and C. S. Ramage, 1976: A technique for estimating tropical open-ocean rainfall from satellite observations. *J. Appl. Meteor.,* **15,** 972–976.

Knutson, T. R., and K. M. Weickmann, 1987: The 30–60 day atmospheric oscillation: Composite life cycles of convection and circulation anomalies. *Mon. Wea. Rev.,* **115,** 1407–1436.

Lau, K. M., and P. H. Chan, 1983: Short-term climate variability and atmospheric teleconnections from satellite-observed outgoing longwave radiation. Part I: Simultaneous relationships. *J. Atmos. Sci.,* **40,** 2735–2750.

——, and ——, 1985: Aspects of the 40–50 day oscillation during the northern winter as inferred from outgoing longwave radiation. *Mon. Wea. Rev.,* **113,** 1889–1909.

——, and ——, 1986a: The 40–50 day oscillation and the El Niño/Southern Oscillation: A new perspective. *Bull. Amer. Meteor. Soc.,* **67,** 533–534.

——, and ——, 1986b: Aspects of the 40–50 day oscillation during the northern summer as inferred from outgoing longwave radiation. *Mon. Wea. Rev.,* **114,** 1354–1367.

——, and ——, 1988: Intraseasonal and interannual variations of tropical convection: A possible link between the 40–50 day oscillation and ENSO? *J. Atmos. Sci.,* **45,** 506–521.

Leary, C. A., and R. A. Houze Jr., 1979: The structure and evolution of convection in a tropical cloud cluster. *J. Atmos. Sci.,* **36,** 437–457.

Liebmann, B., and D. L. Hartmann, 1982: Interannual variations of outgoing IR associated with tropical circulation changes during 1974–1978. *J. Atmos. Sci.,* **39,** 1153–1162.

Lindzen, R. S., and S. Nigam, 1987: On the role of sea surface temperature gradients in forcing low-level winds and convergence in the tropics. *J. Atmos. Sci.,* **44,** 2418–2436.

Manabe, S., D. G. Hahn, and J. L. Holloway, 1974: The seasonal variation of the tropical circulation as simulated by a global model of the atmosphere. *J. Atmos. Sci.,* **31,** 43–83.

Morrissey, M. L., 1986: A statistical analysis of the relationships among rainfall, outgoing longwave radiation and the moisture budget during January–March 1979. *Mon. Wea. Rev.,* **114,** 931–942.

Neelin, J. D., and I. M. Held, 1987: Modeling tropical convergence based on moist static energy budget. *Mon. Wea. Rev.,* **115,** 3–12.

Newell, R. E., 1979: Climate and the Ocean. *Amer. Sci.,* **67,** 405–416.

Ramage, C. S., and A. M. Hori, 1981: Meteorological Aspects of El Niño. *Mon. Wea. Rev.,* **109,** 1827–1835.

Ramanathan, V., and W. Collins, 1991: Thermodynamic regulation of ocean warming by cirrus clouds deduced from observations of the 1987 El Niño. *Nature,* **351,** 27–32.

Rassmusson, E. M., and J. M. Wallace, 1983: Meteorological aspects of the El Niño/Southern oscillation. *Science,* **222,** 1195–1202.

Reynolds, R. W., 1988: A real-time global sea surface temperature analysis. *J. Climate,* **1,** 75–86.

Rossow, W. B., 1989: Measuring cloud properties from space: A review. *J. Climate,* **2,** 201–213.

——, and R. A. Schiffer, 1991: ISCCP cloud data products. *Bull. Amer. Meteor. Soc.,* **72,** 2–20.

——, L. C. Gardner, P. J. Lu, and A. W. Walker, 1991: International Satellite Cloud Climatology Project (ISCCP) Documentation of Cloud Data. WMO/TD-No. 266, World Meteorological Organization, Geneva, 78 pp. plus three appendices.

Somerville, R. C. J., and L. A. Remer, 1984: Cloud optical thickness feedbacks in the CO climate problem. *J. Geophys. Res.,* **89**(D6), 9668–9672.

Waliser, D. E. and N. E. Graham, 1992: Convective cloud complexes and warm-pool SSTs: Coupled interactions and self-regulation. *J. Geophys. Res.,* submitted.

Webster, P. J., 1972: Response of the tropical atmosphere to local steady forcing. *Mon. Wea. Rev.,* **100,** 518–541.

Weickmann, K. M., 1983: Intraseasonal circulation and outgoing longwave radiation modes during northern hemisphere winter. *Mon. Wea. Rev.,* **111,** 1838–1858.

——, G. R. Lussky, and J. E. Kutzbach, 1985: A global-scale analysis of intraseasonal fluctuations of outgoing longwave radiation and 250 mb streamfunction during northern winter. *Mon. Wea. Rev.,* **112,** 941–961.

Welch, R. M., and W. G. Zdunkowski, 1981: The effect of cloud shape on radiative characteristics. *Beitr. Phys. Atmos.,* **54,** 482–491.

Yoo, J.-M., and J. A. Carton, 1988: Outgoing longwave radiation derived rainfall in the tropical Atlantic, with emphasis on 1983–84. *J. Climate,* **1,** 1047–1054.

Zimmerman, P. H., H. B. Selkirk, and R. E. Newell, 1988: The relationship between large-scale vertical motion, highly reflective cloud, and sea surface temperature in the tropical Pacific basin. *J. Geophys. Res.,* **93**(D9), 11 205–11 215.

Zebiak, S. E., 1982: A simple atmospheric model of relevance to El Niño. *J. Atmos. Sci.,* **39,** 2017–2027.

——, 1986: Atmospheric convergence feedback in a simple model for El Niño. *Mon. Wea. Rev.,* **114,** 1263–1271.

——, 1990: Diagnostic studies of Pacific surface winds. *J. Climate,* **3,** 1016–1031.

Zhang, C., 1993: Empirical relationships between sea surface temperature and outgoing longwave radiation over the tropical Pacific Ocean. *J. Climate,*